EUROPEAN ORGANIZATION FOR NUCLEAR RESEARCH (CERN)

CERN-EP-2025-129
2025/08/12

CMS-SUS-24-002

Search for light pseudoscalar boson pairs produced from Higgs boson decays using the 4τ and $2\mu2\tau$ final states in proton-proton collisions at $\sqrt{s} = 13\,\text{TeV}$

The CMS Collaboration*

Abstract

A search for a pair of light pseudoscalar bosons (a_1) produced in the decay of the 125 GeV Higgs boson is presented. The analysis examines decay modes where one a_1 decays into a pair of tau leptons and the other decays into either another pair of tau leptons or a pair of muons. The a_1 boson mass probed in this study ranges from 4 to 15 GeV. The data sample was recorded by the CMS experiment in proton-proton collisions at a center-of-mass energy of 13 TeV and corresponds to an integrated luminosity of $138\,\text{fb}^{-1}$. No excess above standard model (SM) expectations is observed. The study combines the 4τ and $2\mu2\tau$ channels to set upper limits at 95% confidence level (CL) on the product of the Higgs boson production cross section and the branching fraction to the 4τ final state, relative to the Higgs boson production cross section predicted by the SM. In this interpretation, the a_1 boson is assumed to have Yukawa-like couplings to fermions, with coupling strengths proportional to the respective fermion masses. The observed (expected) upper limits range between 0.007 (0.011) and 0.079 (0.066) across the mass range considered. The results are also interpreted in the context of models with two Higgs doublets and an additional complex singlet field (2HD+S). The tightest constraints are obtained for the Type III 2HD+S model. In this case, assuming the Higgs boson production cross section equals the SM prediction, values of the branching ratio for the Higgs boson decay into a pair of a_1 bosons exceeding 16% are excluded at 95% CL for a_1 boson masses between 5 and 15 GeV and $\tan\beta > 2$, with the exception of scenarios in which the a_1 boson mixes with charm or bottom quark-antiquark bound states.

Submitted to the Journal of High Energy Physics

*See Appendix A for the list of collaboration members

1 Introduction

The experimental verification of the standard model (SM), a quantum field theory describing the strong and electroweak interactions between elementary particles, culminated in the discovery of a scalar boson with a mass of 125 GeV by the ATLAS and CMS Collaborations at the CERN LHC [1–3]. Subsequent studies demonstrated that the properties of the discovered boson, denoted henceforth as H, are compatible, at the current level of precision, with the predicted properties of the SM Higgs boson [4, 5].

Despite its striking success in describing the subatomic world, the SM is not considered a complete theory. It does not explain several key phenomena, such as the nature of dark matter, the origin of neutrino masses, and the matter-antimatter asymmetry in the universe. Various extensions to the SM have been proposed to address some of its shortcomings, which include extended Higgs sectors wherein the 125 GeV Higgs boson appears as one of multiple Higgs boson states. Prominent examples of such extensions of the SM are the general two-Higgs-doublet models [6, 7], and the two-Higgs-doublet plus singlet (2HD+S) models, which include an additional complex scalar field [8]. Extended Higgs sectors are also embedded in more elaborate theoretical frameworks, such as the minimal supersymmetric SM (MSSM) [9, 10], which incorporates two Higgs doublets, or the next-to-MSSM (NMSSM) [11, 12], which solves the μ-problem of the MSSM by extending the two Higgs doublets by a complex singlet field [13, 14]. These supersymmetric extensions of the SM provide a candidate for dark matter and introduce additional sources of charge-parity (CP) violation that could explain the observed amount of matter-antimatter asymmetry.

The analysis presented in this paper probes the 2HD+S models, which predict seven physical Higgs boson states: three neutral CP-even, two neutral CP-odd, and two charged bosons. One of the scalars of the neutral sector can be identified as the 125 GeV Higgs boson. At the same time, one of the two pseudoscalars, denoted a_1, can be light enough for $H \to a_1 a_1$ decays to be kinematically possible. Measurements of the Higgs boson couplings so far still allow for a substantial branching fraction of Higgs boson decays to beyond-the-SM particles; the ATLAS and CMS experiments have established upper limits at 95% confidence level (CL) of 12 and 16%, respectively [4, 5]. The search for $H \to a_1 a_1$ decays, therefore, provides an effective probe for possible extensions of the SM and the discovery of new physics phenomena.

The 2HD+S models predict various decay channels for the a_1 boson, with significant branching fractions into fermion pairs. The decay patterns of a_1 bosons are governed by parameters such as the ratio of the vacuum expectation values of the two Higgs doublets ($\tan\beta$) and the a_1 boson mass (m_{a_1}). The different variants of the 2HD+S models—Type I, II, III, and IV—are distinguished by how the Higgs doublets couple to fermions, resulting in distinct decay patterns. Several of these models predict a significant branching fraction of the a_1 boson decay into a pair of tau leptons [8], making this channel a promising avenue for experimental searches.

Numerous searches for $H \to a_1 a_1$ decays have been carried out to date by the ATLAS and CMS Collaborations, exploring different a_1 decay modes, covering the mass range $0.2 < m_{a_1} < 62.5$ GeV [15–33]. The studies did not reveal significant deviations from the SM background expectations, and upper limits were set on the signal rates, thereby constraining the parameters of the 2HD+S models.

In this paper, a search for a light a_1 boson via the decays $H \to a_1 a_1 \to 4\tau$ and $H \to a_1 a_1 \to 2\mu 2\tau$ is presented. The search is based on proton-proton (pp) collision data at a center-of-mass energy of 13 TeV, corresponding to an integrated luminosity of 138 fb^{-1}, recorded by the CMS detector between 2016 and 2018. The analysis covers the m_{a_1} range between 4 and 15 GeV

and employs a specialized strategy to select and identify highly Lorentz-boosted muon or tau lepton pairs with overlapping decay products. Similar searches were performed by the CMS and ATLAS Collaborations [29, 33] using 36 and 140 fb^{-1} of pp collision data, respectively. These searches established upper limits at 95% CL on the Higgs boson production cross section times branching fraction for $\mathrm{H} \to \mathrm{a}_1\mathrm{a}_1 \to 4\tau$, relative to the SM Higgs boson production cross section. The CMS analysis set limits in the range 0.022–0.23, depending on the a_1 boson mass. The ATLAS analysis, based on a larger analyzed data set, placed limits between 0.03 and 0.10. The analysis presented here extends the previous CMS analysis by using approximately four times more data. Moreover, the signal selection criteria have been optimized further, taking advantage of a more precise calibration of the CMS detector achieved towards the end of the LHC Run 2 data-taking period.

The $\mathrm{H} \to \mathrm{a}_1\mathrm{a}_1 \to 4\tau$ decay gives rise to tau leptons that have a lower average transverse momentum (p_T) spectrum compared to the $\mathrm{H} \to \tau\tau$ decay. For about 60% of tau leptons from the signal processes, the visible p_T, defined as the transverse momentum of its detectable decay products, is below 20 GeV. Reconstruction and identification of tau leptons in this kinematic regime is challenging. In particular, the reconstruction of decay modes with neutral pions is hampered by a large flux of low-p_T photons originating from low-energy pp interactions in the same or neighboring bunch crossings (pileup). Conventional CMS algorithms [34] are not optimized for identifying such low-p_T tau leptons, resulting in a rapid degradation of the reconstruction efficiency and purity with decreasing visible p_T. Furthermore, the significant mass difference between the a_1 and Higgs bosons results in a_1 bosons that are highly Lorentz-boosted, and collimated decay products. The resulting overlap of tau leptons from the same a_1 boson further complicates the identification of the $\mathrm{a}_1 \to \tau\tau$ candidates. These challenges are addressed by employing a dedicated search strategy.

The signal topology targeted by the present analysis is illustrated in Fig. 1. The analysis focuses on the $\mathrm{H} \to \mathrm{a}_1\mathrm{a}_1 \to (\tau_\mu\tau_{\text{1-prong}})\,(\tau_\mu\tau_{\text{1-prong}})$ decays, where τ_μ denotes the muonic decay of a tau lepton, and $\tau_{\text{1-prong}}$ stands for its decay into an electron, muon, or one-prong hadronic state. Each a_1 boson is thus identified by the presence of a muon and an additional charged particle nearby. The latter particle is characterized by the presence of one reconstructed track with a charge opposite to that of the muon. Three-prong tau decays are excluded because of their very high quantum chromodynamics (QCD) multijet background and lower reconstruction efficiency. Although the analysis primarily targets the $(\tau_\mu\tau_{\text{1-prong}})(\tau_\mu\tau_{\text{1-prong}})$ decays, the decays $\mathrm{a}_1\mathrm{a}_1 \to (\mu\mu)(\tau_\mu\tau_{\text{1-prong}})$ are also included as they can give rise to a similar topology. The two decay modes are combined to search for the $\mathrm{H} \to \mathrm{a}_1\mathrm{a}_1$ signal, assuming that the a_1 boson has Yukawa-like couplings to fermions, with coupling strengths proportional to the respective fermion masses. Because of its significantly lower branching fraction, the $\mathrm{a}_1\mathrm{a}_1 \to 4\mu$ decay has a negligible contribution to the search sensitivity and is not considered in the present search.

The analysis primarily targets the dominant gluon-gluon fusion (ggF) production mechanism, where the Higgs boson is produced with relatively small p_T and the a_1 bosons are emitted nearly back-to-back in the transverse plane, resulting in a large separation in azimuthal angle ($\Delta\phi$) between the decay products of the two a_1 bosons. When the Higgs boson is produced with high p_T, e.g., due to initial-state radiation in ggF, or through other production mechanisms, the azimuthal angle between the a_1 bosons is reduced, whereas the separation in pseudorapidity ($\Delta\eta$) can still be large. Therefore, the analysis focuses on the identification of same-sign dimuon events with significant angular separation, $\Delta R = \sqrt{(\Delta\phi)^2 + (\Delta\eta)^2}$, where each muon is accompanied by a nearby oppositely charged particle from the same a_1 decay. The requirement of same-sign muons significantly reduces backgrounds from top quark pairs, Drell–Yan processes, and diboson production, thereby enhancing the search sensitivity.

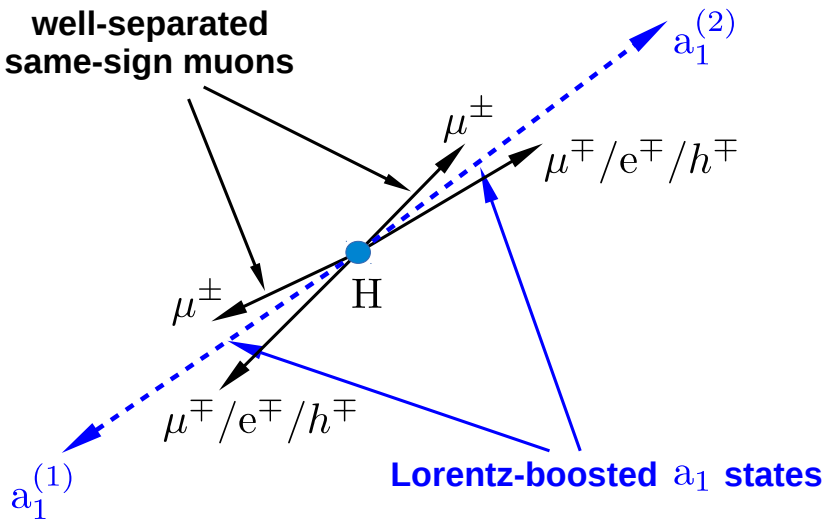

Figure 1: Illustration of the signal topology. The Higgs boson decays into two a_1 bosons, one of which further decays into a pair of tau leptons, and the other into a pair of muons or tau leptons. In the case of $a_1 \to \tau\tau$ decays, one tau lepton is required to decay to a muon, and the other to a single charged particle—either an electron, a muon, or a charged hadron (h). The targeted final state consists of one muon and one oppositely charged track arising from each a_1 boson decay.

Outside the probed mass range of 4–15 GeV, the sensitivity of the present search decreases rapidly. At lower a_1 masses, the background from QCD multijet events overwhelms the signal. At higher masses, the angular separation between the decay products of the a_1 bosons increases, thereby necessitating a different analysis strategy.

Tabulated results are provided in the HEPData record for this analysis [35].

2 The CMS detector

The central feature of the CMS apparatus is a superconducting solenoid of 6 m internal diameter, providing a magnetic field of 3.8 T. Within the solenoid volume are a silicon pixel and strip tracker, a lead tungstate crystal electromagnetic calorimeter (ECAL), and a brass and scintillator hadron calorimeter, each composed of a barrel and two endcap sections. Forward calorimeters extend the pseudorapidity coverage provided by the barrel and endcap detectors. Muons are reconstructed in gas-ionization detectors embedded in the steel flux-return yoke outside the solenoid. More detailed descriptions of the CMS detector, together with a definition of the coordinate system used and the relevant kinematic variables, can be found in Refs. [36, 37].

Events of interest are selected using a two-tiered trigger system. The first level (L1), composed of custom hardware processors, uses information from the calorimeters and muon detectors to select events at a rate of around 100 kHz within a fixed latency of about 4 μs [38]. The second level, known as the high-level trigger, consists of a farm of processors running a version of the full event reconstruction software optimized for fast processing, which reduces the event rate to around 1 kHz before data storage [39, 40].

3 Simulated samples

The signal events for the $H \to a_1 a_1 \to 4\tau$ channel are simulated at leading order (LO) using the PYTHIA (v.8.212) event generator [41], targeting three major Higgs boson production mechanisms: ggF, vector boson fusion (VBF), and Higgs-strahlung (VH). For the $H \to a_1 a_1 \to 2\mu 2\tau$ decay channel, events are generated at LO for the dominant ggF production mode with MADGRAPH5_aMC@NLO (v.2.6.5) [42]. The acceptance of the $H \to a_1 a_1 \to 2\mu 2\tau$ signal is corrected to account for subdominant contributions from the VBF and VH processes as detailed in Section 5. Simulation studies have demonstrated that the signal acceptance is highly sensitive to the p_T spectrum of the Higgs boson. Therefore, the signal samples generated at LO are reweighted to match the Higgs boson p_T spectrum predicted by theoretical computations that incorporate higher-order corrections. The p_T distribution of the Higgs boson produced via ggF is reweighted for both decay channels (4τ and $2\mu 2\tau$) using *K*-factors calculated with the program HqT (v.2.0) [43, 44], which computes the p_T spectrum of the Higgs boson at next-to-LO (NLO) with next-to-next-to-leading-logarithmic resummation at low p_T. For VBF and VH processes, the p_T distribution of the Higgs boson is reweighted using *K*-factors calculated with the NLO POWHEGBOX (v.2.0) event generator [45–47].

The major source of background for the analysis is QCD multijet production, followed by subdominant contributions from Drell–Yan processes with Z or W boson production accompanied by jets (Z+jets and W+jets), top quark-antiquark pair production with additional jets ($t\bar{t}$+jets), single top quark production, and vector boson pair production (diboson). The QCD multijet and diboson backgrounds are simulated using PYTHIA (v.8.212), whereas the Z+jets and W+jets backgrounds are generated at LO with MADGRAPH5_aMC@NLO (v.2.6.5). The single top quark and $t\bar{t}$+jets processes are generated at NLO using POWHEGBOX (v.2.0).

Parton showering and fragmentation for all Monte Carlo (MC) samples are executed using PYTHIA (v.8.212). The CP5 tune is applied to describe the underlying event [48]. All simulated samples utilize the NNLO NNPDF3.1 PDFs. For samples produced at LO with MADGRAPH5_aMC@NLO, the MLM jet matching scheme is employed [49]. The detector response is simulated with the GEANT4 package [50, 51]. The contribution of pileup is replicated by simulation of minimum bias interactions, which are then superimposed on the primary hard-scattering event. The simulated events are then reweighted to reflect the observed pileup distribution in the experimental data. The average number of pileup collisions was 27 (38) in the 2016 (2017–2018) data.

4 Event reconstruction

Events containing two muon candidates and two additional tracks are selected in the analysis. Track reconstruction is performed using the combinatorial track finder algorithm [52], which employs Kalman filtering to refine the track estimates; the analysis selects the "high-purity" tracks defined in Section 4.4 of Ref. [52].

The primary vertex (PV) is identified as the vertex corresponding to the hardest scattering in the event, evaluated using tracking information alone, as described in Section 9.4.1 of Ref. [53].

The particle-flow (PF) algorithm [54] reconstructs and identifies individual particles (PF candidates) in an event using combined information from the various elements of the CMS detector. Muons are identified as tracks in the central tracker consistent with either a track or several hits in the muon system and associated with calorimeter deposits compatible with the expectation for minimum-ionizing particles. These PF muons are further required to pass dedicated

identification requirements, which depend on several parameters, including track quality, impact parameter significance, and number of muon chamber hits, to suppress contributions from nonprompt decays of hadrons into muons and their punchthrough to the muon detectors. The analysis employs the medium identification criterion [55], which yields an overall efficiency of 98–99% for muons with $p_T > 20\,\text{GeV}$. Scale factors, derived by comparing the muon identification efficiencies between data and simulation, are applied to the MC samples to match the performance observed in data.

Jets are reconstructed by clustering PF candidates using the anti-k_T algorithm [56, 57] with a distance parameter of 0.4. Charged particles not associated with the PV are excluded from the clustering using the charged hadron subtraction method [54]. The reconstructed jet energies are corrected in both data and simulation to account for effects from nonlinear detector response and contamination from pileup [58]. The jet energy resolution is corrected in simulation to improve the agreement with data.

Jets resulting from the fragmentation and hadronization of bottom quarks (b jets) are identified using the DEEPJET algorithm [59, 60], and labeled as b-tagged. The tight working point of the b tagging discriminator is used, which corresponds to a rate of 0.1% for misidentifying a light jet, i.e., a gluon or light-quark jet, as a b jet [61]. The corresponding b tagging efficiency, measured from $\mathrm{t\bar{t}}$+jets events, is around 65%.

5 Event selection

The search, targeting nonisolated same-sign muon pairs, requires a specialized triggering strategy. Events of interest are recorded using a set of dimuon triggers. In 2016 and 2017, the trigger required the highest-p_T (leading) and second-highest-p_T (subleading) muons to have transverse momenta of at least 17 and 8 GeV, respectively. In 2018, the thresholds were raised to 18 and 9 GeV, respectively. Additionally, in 2016 and 2018, the trigger required the two muons to have the same charge. In 2016, it was also required that the two muon tracks have their points of closest approach to the beam axis within 0.2 cm of each other along the z direction. The triggers employed in 2016 and 2018 did not impose any isolation requirements on the muons. However, in 2017, a nonisolated same-sign dimuon trigger was not available. Thus, a dimuon trigger imposing a loose isolation criterion on both muons was used instead. This criterion required the ratio of the p_T sum of charged hadrons, within an isolation cone of size $\Delta R = 0.3$ around the muon, to the p_T of the muon to be less than 0.4. Even with this requirement, the trigger was efficient in selecting the signal with a relative loss of efficiency, estimated from simulation studies, ranging from 5% at $m_{a_1} = 15\,\text{GeV}$ to 20% at $m_{a_1} = 4\,\text{GeV}$.

As the first step in the offline selection, a b jet veto is imposed, rejecting events that contain one or more b-tagged jets with $p_T > 20\,\text{GeV}$ and $|\eta| < 2.4$. This veto is essential to suppress background from QCD multijet events with heavy-flavor hadrons that decay into muons. The remaining events that pass the trigger selection criteria are required to contain at least two same-sign muons, each having $|\eta| < 2.4$. The p_T of the leading and subleading muon is required to be greater than 19 and 10 GeV, respectively. The transverse (longitudinal) impact parameter of the muons with respect to the PV is required to be $|d_0| < 0.05$ ($|d_z| < 0.1$) cm. The angular separation between the muons must be $\Delta R > 1.5$. If more than one pair of same-sign muons meets these criteria, the pair with the highest scalar sum of p_T is selected.

The next selection step employs information from the tracks associated with the reconstructed charged PF objects, excluding the pair of same-sign muons. This information is used to identify and isolate the candidates for the $a_1 \to \tau_\mu \tau_{1\text{-prong}}$ or $a_1 \to \mu\mu$ decays, hereafter referred to as

a_1 candidates. Two types of tracks are considered, namely "isolation" and "signal" tracks. The signal tracks are a subset of the isolation tracks, subject to stricter selection criteria. The purpose of each track type and their selection criteria are given in Table 1.

Table 1: The purpose and selection criteria for the two types of tracks used in the selection procedure.

Type of track	p_T	$\|\eta\|$	$\|d_0\|$	$\|d_z\|$	Purpose
Isolation	>1.0 GeV	<2.4	<0.2 cm	<0.3 cm	Provides the isolation criteria for muon candidates
Signal	>2.5 GeV	<2.4	<0.02 cm	<0.04 cm	Used together with muons to construct a_1 candidates

Each selected muon of the same-sign muon pair is required to have exactly one isolation track within a ΔR cone of 0.5 around the muon. The background components, especially QCD multijet events, tend to have higher track multiplicity with respect to the signal and, hence, are rejected by imposing the isolation requirement. A muon+track system is accepted as an a_1 candidate if the isolation track around the muon meets the signal track criteria. The event is selected in the final sample if it contains two a_1 candidates. The set of selection requirements outlined above defines the signal region (*SR*).

The number of observed events selected in the *SR* is 7803. Simulation studies indicate that QCD multijet events are the predominant background in the *SR*. Contributions from other backgrounds only comprise about 1% of the selected events in the *SR*. In Table 2, the expected signal acceptance times selection efficiency ($\mathcal{A}\epsilon$), and the expected yield of signal events in the *SR* from simulation are reported for a few representative values of m_{a_1}. For each of the two considered decay channels, 4τ and $2\mu 2\tau$, the value of $\mathcal{A}\epsilon$ is evaluated as the expected yield of signal events from simulation relative to the total number of signal events expected in the respective decay channel. The expected signal yields are calculated assuming a benchmark value of the branching fraction, $\mathcal{B}(H \to a_1 a_1)\mathcal{B}^2(a_1 \to \tau\tau) = 0.05$, and the SM predictions for the Higgs boson production cross sections: 48.58 pb for ggF, 3.78 pb for VBF, and 2.26 pb for VH [62]. The contributions from the ggF, VBF, and VH processes are summed to determine the 4τ yield. The expected $2\mu 2\tau$ signal yield is estimated under the assumption that the a_1 boson has Yukawa-like couplings to fermions, with coupling strengths proportional to the fermion masses. Under this assumption, the ratio of the $a_1 \to \mu\mu$ and $a_1 \to \tau\tau$ partial widths satisfies the relation [63]

$$\frac{\Gamma(a_1 \to \mu\mu)}{\Gamma(a_1 \to \tau\tau)} = \frac{m_\mu^2}{m_\tau^2} \frac{\sqrt{1 - \left(2m_\mu/m_{a_1}\right)^2}}{\sqrt{1 - \left(2m_\tau/m_{a_1}\right)^2}}. \tag{1}$$

Using Eq. (1), the ratio of the branching fractions for $a_1 a_1 \to 2\mu 2\tau$ and $a_1 a_1 \to 4\tau$ decays is computed as

$$\frac{\mathcal{B}(a_1 a_1 \to 2\mu 2\tau)}{\mathcal{B}(a_1 a_1 \to 4\tau)} = 2\frac{\mathcal{B}(a_1 \to \mu\mu)}{\mathcal{B}(a_1 \to \tau\tau)} = 2\frac{\Gamma(a_1 \to \mu\mu)}{\Gamma(a_1 \to \tau\tau)}. \tag{2}$$

The factor of 2 in Eq. (2) accounts for the possibility of either a_1 boson decaying into $\mu\mu$ or $\tau\tau$. The value of the ratio in Eq. (2) decreases from 0.016 at $m_{a_1} = 4$ GeV to 0.0073 at $m_{a_1} = 15$ GeV. To account for subdominant contributions to the $2\mu 2\tau$ final state from VBF and VH production, the ratios of $\mathcal{A}\epsilon$ between the $2\mu 2\tau$ and 4τ channels are assumed to be identical across

all production mechanisms. The value of $\mathcal{A}\epsilon$ for the ggF process is then scaled accordingly to estimate the total $2\mu2\tau$ yield. This assumption has been verified with simulated signal samples for two representative mass hypotheses of $m_{a_1} = 5$ and 10 GeV. For both masses, the values of $\mathcal{A}\epsilon$ for the two decay channels are found to be consistent within 3–5%.

Table 2: Signal acceptance times selection efficiency $\mathcal{A}\epsilon$, defined in the text, and the number of expected signal events after selection in the *SR*, computed using simulated signal samples for representative mass hypotheses. The Higgs boson cross sections from ggF, VBF, and VH production mechanisms are set to the SM predictions [62]. The number of expected signal events is computed for a benchmark value of the branching fraction $\mathcal{B}(H \to a_1 a_1)\mathcal{B}^2(a_1 \to \tau\tau) = 0.05$. The quoted uncertainties in the predictions from simulation include only the statistical component. In data, 7803 events are selected in the *SR*.

Signal	$\mathcal{A}\epsilon$ [10^{-4}]		Expected signal yield	
m_{a_1} [GeV]	4τ	$2\mu2\tau$	4τ	$2\mu2\tau$
5	3.52 ± 0.10	103 ± 2	134 ± 4	39.7 ± 0.4
8	2.55 ± 0.09	76.0 ± 1.0	97.2 ± 3.3	23.0 ± 0.3
12	1.37 ± 0.06	35.6 ± 0.7	52.1 ± 2.4	10.1 ± 0.2
15	0.32 ± 0.03	7.5 ± 0.3	12.3 ± 1.1	2.1 ± 0.1

6 Final discriminant

A two-dimensional (2D) distribution of the invariant masses of the muon+track systems constituting the a_1 candidates is chosen as the final discriminant and employed to distinguish between signal and background. This 2D distribution is populated with pairs of muon+track invariant masses (m_1, m_2), ordered by their value, $m_2 > m_1$. Figure 2 illustrates the binning of the 2D distribution. Each bin is labeled (i, j), where i and j denote the bin indices along the m_1 and m_2 axes, respectively. Since m_2 is required to be greater than m_1, only the bins (i, j) where $j \geq i$ are filled, resulting in a total of $6(6+1)/2 = 21$ independent bins. The bin boundaries along each axis are at 0, 1, 2, 3, 4, and 5.2 GeV. Bins $(i, 6)$ with $i = 1, \ldots, 5$ include all events with $m_2 > 5.2$ GeV, while bin $(6, 6)$ contains all events with m_1 and $m_2 > 5.2$ GeV. The binning is optimized to achieve the highest sensitivity to the signal for all tested mass hypotheses of a_1 while ensuring reliable and robust estimation of the background, as detailed in Section 7. With the chosen binning, the statistical uncertainty in the background estimate is kept between 1 and 40% across all bins of the (m_1, m_2) distribution.

7 Background modeling

As mentioned in Section 5, QCD multijets constitute the dominant source of background, with small contributions coming from processes such as $t\bar{t}$, Z+jets, W+jets, and diboson production. To model the shape of the (m_1, m_2) distribution of the background in the *SR*, a binned template is constructed as:

$$f_{2D}(i, j) = C(i, j)\,[f_{1D}(i)\, f_{1D}(j)]^{\text{sym}}, \tag{3}$$

where

- $f_{2D}(i, j)$ represents the content of bin (i, j) in the (m_1, m_2) distribution, normalized to unity.

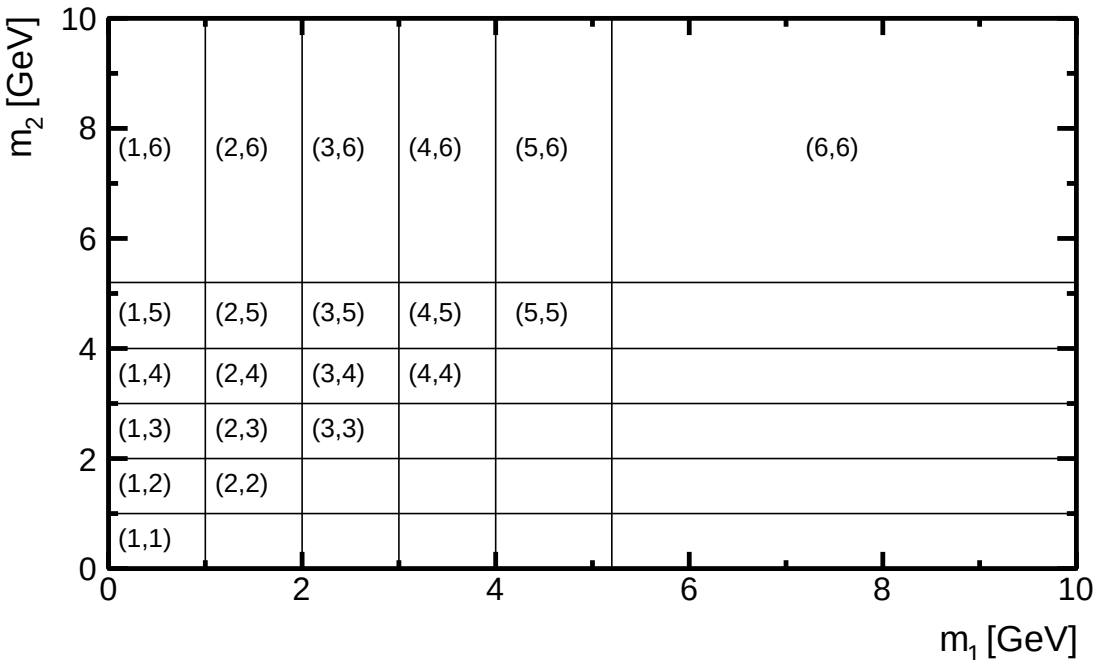

Figure 2: Binning of the 2D (m_1, m_2) distribution. Each bin is labeled (i, j), where i is the bin index along m_1 (x axis) and j is the bin index along m_2 (y axis). Bins $(i, 6)$ with $i = 1, ..., 5$ include all events with $m_2 > 5.2\,\text{GeV}$, while bin $(6, 6)$ contains all events with m_1 and $m_2 > 5.2\,\text{GeV}$.

- $f_{1D}(i)$ is the content of bin i in the one-dimensional (1D) muon+track invariant mass distribution, normalized to unity. Each event contributes two entries to this distribution.
- $C(i, j)$ is a symmetric matrix, accounting for possible correlation between m_1 and m_2. The condition $C(i, j) = 1$ for all bins (i, j) would indicate an absence of correlation between m_1 and m_2. The elements of the matrix $C(i, j)$ are referred to as "correlation factors" henceforth.

Equation (3) includes a symmetrization operation, denoted by 'sym', which is applied to the product of the 1D distributions $f_{1D}(i)$ and $f_{1D}(j)$ and defined as follows:

$$[f_{1D}(i)\, f_{1D}(j)]^{\text{sym}} = \begin{cases} 2 f_{1D}(i)\, f_{1D}(j), & \text{if } i \neq j, \\ f_{1D}(i)\, f_{1D}(i), & \text{if } i = j. \end{cases} \tag{4}$$

This symmetrization ensures that the contributions from the nondiagonal bins (i, j) and (j, i) in the Cartesian product $f_{1D}(i) f_{1D}(j)$ are correctly accounted for in the 2D (m_1, m_2) distribution, given the ordering imposed on the muon+track invariant masses. The normalization of the background is left unconstrained prior to the signal extraction.

In order to derive and validate the modeling of $f_{1D}(i)$ and $C(i, j)$, multiple control regions (*CR*s), disjoint from the *SR*, are defined based on variations in the isolation criteria applied to one or both muon+track pairs. The isolation criteria are defined by the number of tracks within a cone of $\Delta R = 0.5$ around the muon momentum direction. The two muons are labeled as "first muon" and "second muon". The first muon serves as a "probe" used to assess $f_{1D}(i)$ as a function of the isolation criteria of the second muon, the "tag", as described in Section 7.1 below. In the *CR* labeled "*CR Loose-Iso*" which is employed to derive the $C(i, j)$, both muons play the role of probes. A summary of the *CR*s and *SR*, along with the specifications for the

first and second muon, is presented in Table 3. Detailed definition of the *CR*s is provided in Sections 7.1 and 7.2. In all *CR*s, the expected signal contamination constitutes 0.1–1% (0.5–6%) of the background yield across all bins of the $f_{1D}(i)$ ($f_{2D}(i,j)$) distributions for all tested a_1 boson mass hypotheses, and thus has negligible impact on the background modeling and final result.

Table 3: Definition of the *CR*s used to construct and validate the background model. The last row defines the *SR*. The symbols N_{iso} and N_{sig} denote the number of isolation and signal tracks, respectively, within a cone of $\Delta R = 0.5$ around the muon momentum direction. In cases where N_{sig} is not mentioned, there is no explicit requirement on the number of signal tracks.

Region	First μ	Second μ	Purpose
CR N_{23}	$N_{sig} = 1$, $N_{iso} = 1$	$N_{iso} = 2, 3$	Determination of $f_{1D}(i)$
CR $N_{iso,1}$	$N_{sig} \geq 1$, $N_{iso} > 1$	$N_{sig} = 1$, $N_{iso} = 1$	Validation and systematic
CR $N_{iso,23}$	$N_{sig} \geq 1$, $N_{iso} > 1$	$N_{iso} = 2, 3$	uncertainty estimate of $f_{1D}(i)$
CR Loose-Iso	$N_{sig} = 1, N_{iso} = 3, 4$	$N_{sig} = 1, N_{iso} = 3, 4$	Determination of $C(i,j)$
SR	$N_{sig} = 1$, $N_{iso} = 1$	$N_{sig} = 1$, $N_{iso} = 1$	Signal extraction

7.1 Modeling of $f_{1D}(i)$

The $f_{1D}(i)$ distribution is modeled using the *CR* labeled "*CR* N_{23}". This *CR* comprises events that pass the same-sign dimuon selection criteria and include only one a_1 candidate, formed by an isolated signal track and a muon (referred to as the first muon). The invariant mass of this first muon and its associated track is used to construct the $f_{1D}(i)$ distribution. The second muon in the event must be accompanied by either two or three nearby isolation tracks. Simulations indicate that *CR* N_{23} is enriched in QCD events, with less than 5% of the events coming from non-QCD backgrounds. The modeling of $f_{1D}(i)$ is based on the assumption that the kinematic distributions of the muon+track system forming the a_1 candidate are weakly affected by the isolation criteria applied to the second muon, therefore implying that the $f_{1D}(i)$ distribution in the *SR* is similar to that in *CR* N_{23}.

A direct test of this assumption is not conclusive because of the limited size of simulated samples. Therefore, the hypothesis is verified using additional *CR*s labeled "*CR* $N_{iso,1}$" and "*CR* $N_{iso,23}$". Events are selected in these *CR*s if the first muon has more than one isolation track, and at least one of these isolation tracks also fulfils the criteria for signal tracks. Since more than one of these tracks can pass the signal track requirements, two scenarios are evaluated, using either the signal track with the lowest p_T ("softest") or the highest p_T ("hardest") to compute the muon+track invariant mass. If only one signal track is found around the first muon, it serves as both the "softest" and "hardest" track. The two control regions differ in the isolation criteria applied to the second muon: *CR* $N_{iso,1}$ selects events where the second muon has exactly one signal track, matching the isolation condition in the *SR*, while *CR* $N_{iso,23}$ selects events where it has two or three isolation tracks, similar to *CR* N_{23}. The invariant mass distributions of the first muon and its softest or hardest accompanying track are then compared between the two different isolation scenarios of the second muon. The results of this study are presented in Fig. 3. In both cases, the invariant mass distributions differ in each bin by less than 7%, suggesting that the invariant mass of the muon+track system forming an a_1 candidate is not highly sensitive to the isolation requirement on the second muon. To address any system-

atic effects on the modeling of the $f_{1D}(i)$ distribution in *CR* N_{23}, the observed differences are treated as a shape uncertainty in the normalized $f_{1D}(i)$ template.

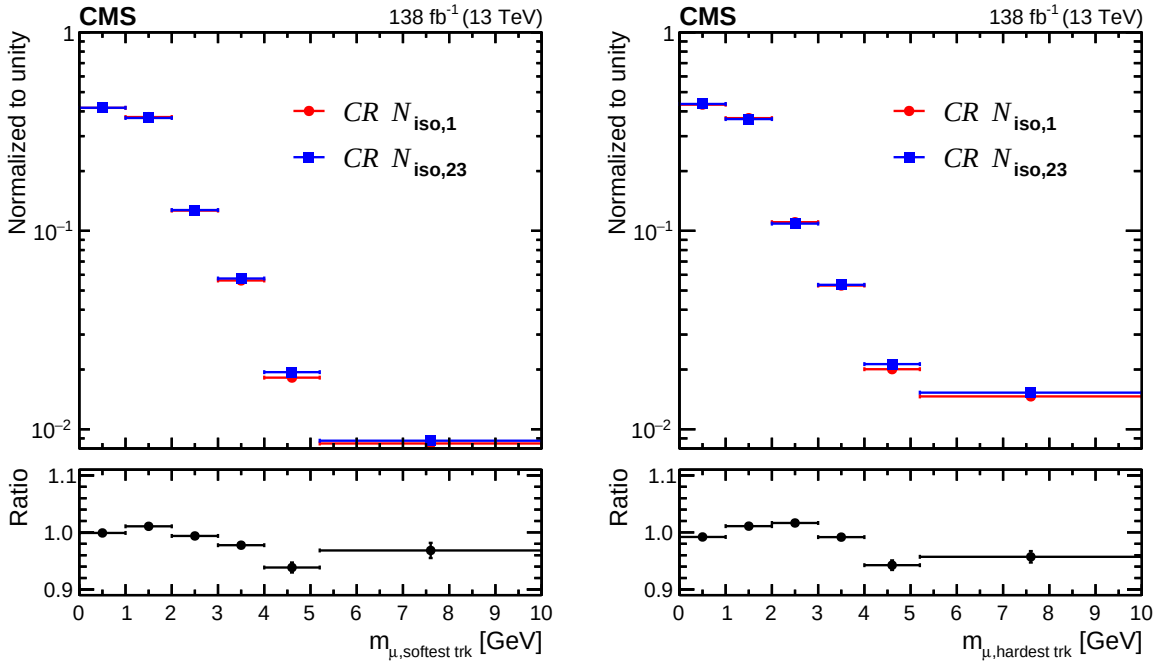

Figure 3: The observed invariant mass distribution, normalized to unity, of the first muon and the softest (left) or hardest (right) accompanying signal track for different isolation requirements imposed on the second muon: one isolation track (*CR* $N_{\text{iso},1}$; circles) or two to three isolation tracks (*CR* $N_{\text{iso},23}$; squares). Vertical bars represent statistical uncertainties, which are smaller than the marker size in most cases and thus imperceptible. The horizontal bars show the bin width. The lower panels show the ratio of the distribution in *CR* $N_{\text{iso},23}$ to that in *CR* $N_{\text{iso},1}$. The last bin in both distributions includes all entries with invariant mass of the muon+track system greater than 5.2 GeV.

Figure 4 presents the muon+track invariant mass distribution, normalized to unity, for data selected in the *SR* and for the background model derived from *CR* N_{23}. The data and background distributions are compared to the signal distributions obtained from simulation for four representative mass hypotheses, m_{a_1} = 5, 8, 12, and 15 GeV. The signal distributions include both the 4τ and $2\mu 2\tau$ contributions. Each distribution contains two entries per event, corresponding to the two selected muon+track systems. The invariant mass of the muon+track system demonstrates higher discrimination power between the background and the signal at higher m_{a_1}. For lower masses, the signal shape becomes more similar to the background.

7.2 Modeling of $C(i,j)$

The correlation factors $C(i,j)$ are determined using a different *CR*, labeled "*CR Loose-Iso*", which does not overlap with the *SR*. This *CR* consists of events containing two same-sign muons that meet the identification and kinematic selection criteria detailed in Section 5. In *CR Loose-Iso*, each muon must have three or four nearby tracks, one of which must be a signal track and the rest are isolation tracks. Simulations predict that QCD multijet events comprise approximately 99% of the events in this *CR*. The events in this *CR* are used to construct $f_{2D}(i,j)$, and the

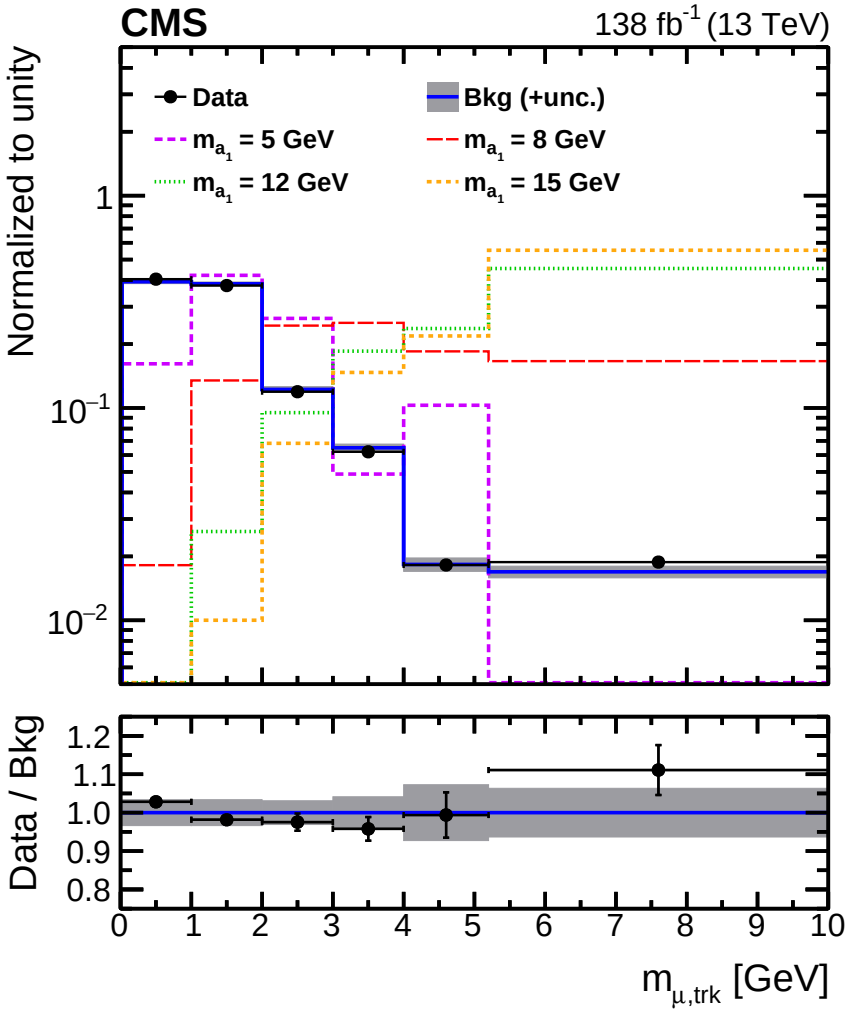

Figure 4: Invariant mass distribution of the muon+track pair, normalized to unity, for events passing the signal selection. Events in data are represented by black points with the vertical bars representing the statistical uncertainty and the horizontal bars the bin width. The expected background distribution derived from *CR* N_{23} is shown by the solid blue histogram, with the grey band giving the uncertainty in the background prediction, including systematic and statistical components. Also shown are normalized distributions from signal simulations for four mass hypotheses, m_{a_1} = 5, 8, 12, and 15 GeV (dashed colored histograms). The lower panel displays the ratio of the data to the expected background.

correlation factors $C(i,j)$ are then derived using Eq. (3) as:

$$C(i,j) = \frac{f_{2D}(i,j)}{[f_{1D}(i)\, f_{1D}(j)]^{\text{sym}}}. \tag{5}$$

where $f_{1D}(i)$ is the 1D normalized distribution with two entries per event. Figure 5 shows the correlation factors $C(i,j)^{CR}_{\text{data}}$ obtained from the data in *CR Loose-Iso*.

To estimate $C(i,j)$ in data in the *SR*, the correlation factors derived with data in *CR Loose-Iso* are corrected for the difference in $C(i,j)$ between the *SR* and the *CR Loose-Iso* by comparing samples of simulated background events. The correlation factors estimated from simulation in the *SR*, $C(i,j)^{CR}_{\text{MC}}$, and *CR Loose-Iso*, $C(i,j)^{CR}_{\text{MC}}$, are shown in Fig. 6.

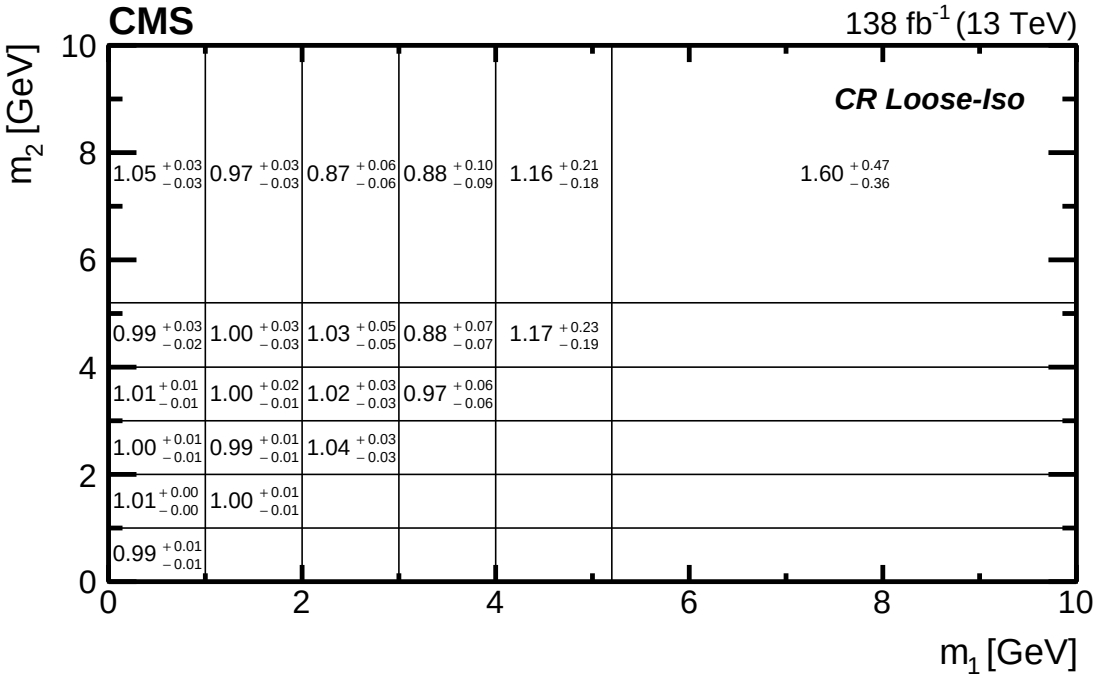

Figure 5: The correlation factors $C(i,j)^{CR}_{\text{data}}$ with their statistical uncertainties.

The correlation factors in data in the *SR*, $C(i,j)^{SR}_{\text{data}}$, are then computed as

$$C(i,j)^{SR}_{\text{data}} = C(i,j)^{CR}_{\text{data}} \frac{C(i,j)^{SR}_{\text{MC}}}{C(i,j)^{CR}_{\text{MC}}}, \tag{6}$$

Finally, the $C(i,j)^{CR}_{\text{data}}$ values are multiplied by a common scale factor of 1.02 to ensure that the $f_{\text{2D}}(i,j)$ terms in the *SR* add up to unity, according to Eq. (3). This scale factor does not affect the final result, as the overall normalization of the background is left unconstrained prior to the signal extraction.

8 Signal modeling

The signal model template is constructed using simulated samples of $\text{H} \to \text{a}_1\text{a}_1 \to 4\tau$ and $2\mu 2\tau$ decays. The analysis measures the signal strength modifier, defined as the product of the measured signal cross section times branching fraction, $\mathcal{B}(\text{H} \to \text{a}_1\text{a}_1)\mathcal{B}^2(\text{a}_1 \to \tau\tau)$, relative to the value predicted by the SM for the inclusive Higgs boson production cross section. The relative contributions from different Higgs boson production modes are determined by the corresponding cross sections predicted by the SM. The contribution from the $\text{H} \to \text{a}_1\text{a}_1 \to 2\mu 2\tau$ decay is computed under the assumption that the partial widths of the $\text{a}_1 \to \tau\tau$ and $\text{a}_1 \to \mu\mu$ decays satisfy Eq. (1).

The muon+track invariant mass distribution in the $\text{a}_1 \to \mu\mu$ decay channel peaks at the nominal a_1 mass. In contrast, the reconstructed mass of the muon+track system in the $\text{a}_1 \to \tau\tau$ decay is generally lower and has a larger dispersion due to the presence of undetected neutrinos. As a result, the (m_1, m_2) distribution for simulated $2\mu 2\tau$ events has a considerably different shape than that for 4τ events. Figure 7 illustrates the (m_1, m_2) distributions, unrolled into a 1D array, for the 4τ and $2\mu 2\tau$ simulated events with $m_{\text{a}_1} = 5$, 8, 12, and 15 GeV. The distributions

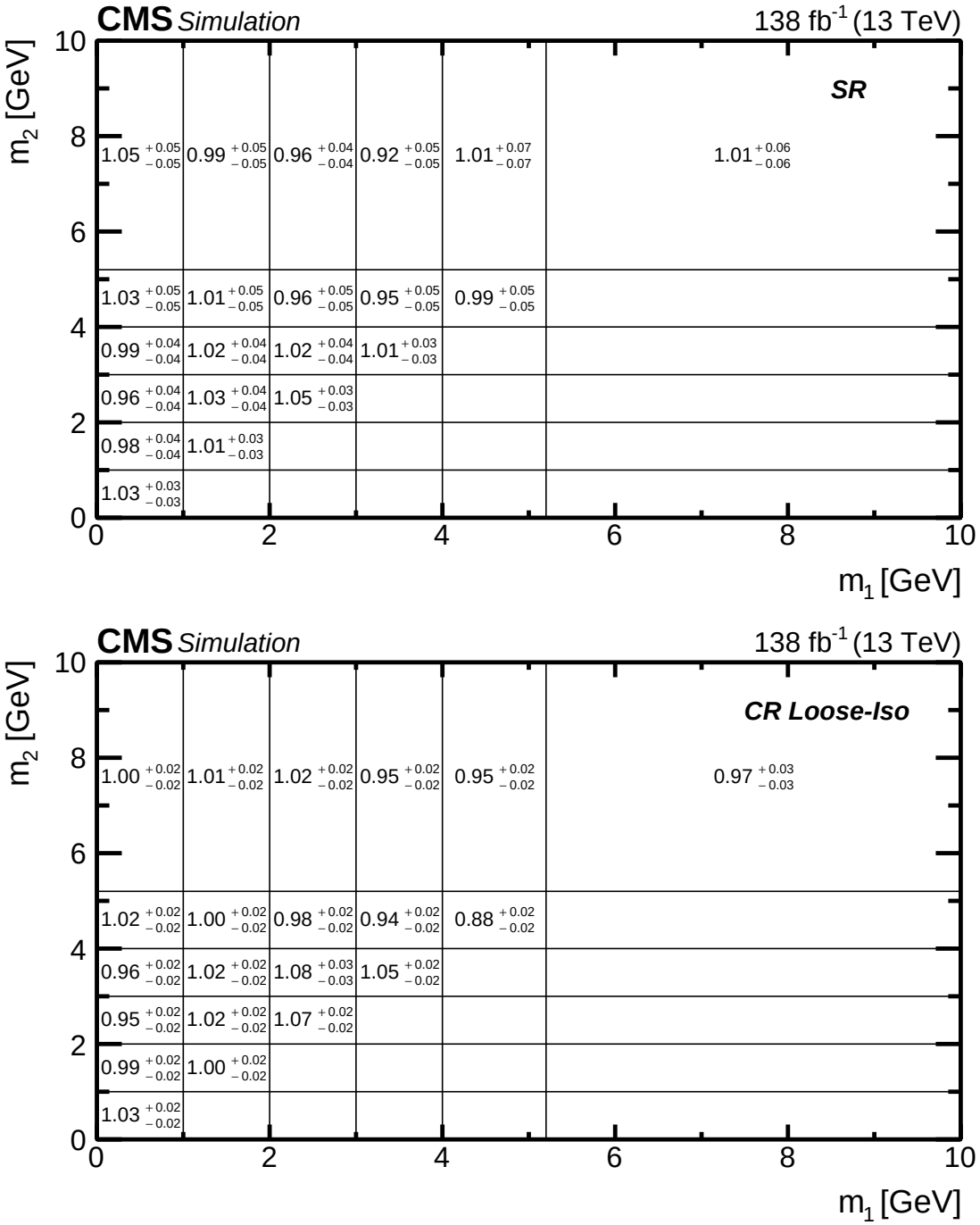

Figure 6: The correlation factors $C(i,j)^{CR}_{\mathrm{MC}}$ (top) and $C(i,j)^{CR}_{\mathrm{MC}}$ (bottom) with their statistical uncertainties.

are normalized assuming the SM Higgs boson production rate and $\mathcal{B}(\mathrm{H} \to \mathrm{a_1 a_1})\mathcal{B}^2(\mathrm{a_1} \to \tau\tau) = 0.05$.

9 Systematic uncertainties

Several sources of uncertainty of both statistical and systematic origins are considered in the analysis. A summary of the uncertainties is provided in Table 4. Statistical uncertainties arise

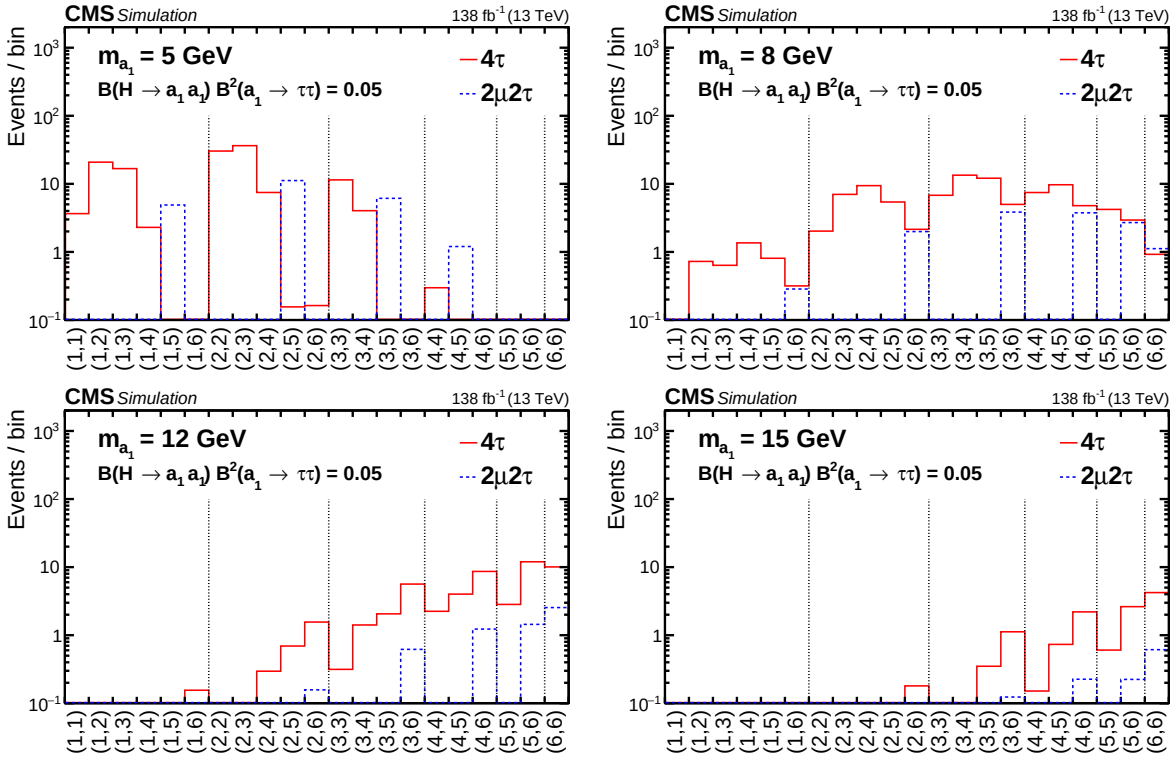

Figure 7: The simulated signal (m_1, m_2) distribution, converted into a 1D array, for m_{a_1} values of 5 (upper left), 8 (upper right), 12 (lower left), and 15 GeV (lower right). The contributions of the $H \to a_1 a_1 \to 4\tau$ (red histograms) and $2\mu 2\tau$ (blue histograms) decays are shown. The distributions are normalized assuming SM Higgs production cross section and $\mathcal{B}(H \to a_1 a_1)\mathcal{B}^2(a_1 \to \tau\tau) = 0.05$. The bin notation follows that of Fig. 2.

from the limited size of the data samples in the *CR*s and of the simulated signal samples. These uncertainties are incorporated into the analysis on a bin-by-bin basis using the Barlow–Beeston "lite" method [64]. Various systematic uncertainties are included, classified into two categories: background-related and signal-related.

9.1 Uncertainties related to background

The shape of the background in the (m_1, m_2) distribution is modeled according to Eq. (3). This distribution is affected by the shape uncertainty in $f_{1D}(i)$, described in Section 7.1, which accounts for potential biases introduced by estimating the 1D distribution in *CR* N_{23}. The uncertainty, derived by comparing $f_{1D}(i)$ between *CR* $N_{iso,1}$ and *CR* $N_{iso,23}$, is found to vary from 2–7% across individual bins of $f_{1D}(i)$. These variations are propagated to $f_{2D}(i,j)$ in Eq. (3) via six nuisance parameters, one per bin of the $f_{1D}(i)$ template.

The background shape is further impacted by uncertainties related to the extrapolation of $C(i,j)$ from *CR Loose-Iso* to the *SR* using simulated background samples. Variations in the modeling of initial- and final-state radiation (ISR and FSR) during parton showering can impact the reconstructed muon+track invariant masses and their correlations in events where an a_1 candidate is mimicked by a hadronic jet, thus leading to potential deviations in $C(i,j)$. To account for this, the ISR and FSR parton shower scales are varied independently up and down by a factor of 2. These variations change the estimate of $C(i,j)$ in *CR Loose-Iso* and the *SR* by 0.5–3% depending on (i,j). Uncertainties in the estimate of $C(i,j)$ also arise from limited understanding of contributions from non-QCD events. The non-QCD background fraction is varied by

Table 4: Summary of systematic uncertainties affecting the estimation of signal and background. The terms ISR and FSR refer to initial- and final-state radiation, and the symbols μ_R and μ_F denote the renormalization and factorization scales, respectively. The impact of shape-altering and bin-by-bin uncertainties is quoted in terms of relative variations of yields across all bins of the modeled (m_1, m_2) distributions. For the normalization (norm.) uncertainties, the impact on the overall estimated yield is reported. The last column indicates how a given uncertainty is correlated across the data-taking years. Bin-by-bin statistical uncertainties for simulated signal samples are quoted for the most populated bins containing 80% of the total yield of selected signal events.

Source	Type	Value	Correlated
Uncertainties affecting background estimate			
Modeling of $f_{1D}(i)$ in *CR*s	shape	2–7%	no
ISR/FSR scales	shape	1–2%	yes
Non-QCD contribution	shape	6%	yes
Limited size of data samples in *CR*s	bin-by-bin	1–40%	no
Uncertainties affecting signal estimate			
Integrated luminosity	norm.	<3%	partially
Muon ID and trigger efficiency	norm.	3%	yes
Track ID/isolation efficiency	shape	10–20%	no
Prefiring weights	norm.	<3%	no
b tagging	norm.	<0.5%	partially
Limited size of simulated samples	bin-by-bin	1–2%	no
μ_R and μ_F scales ($\mathcal{A}\epsilon$)	norm.	1–3%	yes
μ_R and μ_F scales (cross sections)	norm.	1–5%	yes
PDF ($\mathcal{A}\epsilon$)	norm.	1–2%	yes
PDF (cross sections)	norm.	1–3%	yes

$\pm 50\%$, leading to variations between 0.2 and 5% across (i, j). Shape-altering uncertainties in the estimation of $C(i,j)^{CR}_{\text{data}}$ are incorporated by varying the correlation factors $C(i,j)^{CR}_{\text{MC}}$ and $C(i,j)^{CR}_{\text{MC}}$ based on the aforementioned systematic shifts. The associated shape uncertainties are determined by comparing the correlation factors derived from simulated events in the *SR* and *CR Loose-Iso* after applying these systematic variations. Overall, the systematic uncertainties associated with ISR, FSR, and non-QCD contributions induce variations of up to 1, 2, and 6%, respectively, in the background yields for individual bins. Other uncertainties related to the simulation of background samples have a negligible impact on $C(i, j)$ and affect the final results only marginally.

9.2 Uncertainties related to signal

The integrated luminosities for the data-taking years 2016, 2017, and 2018 have individual uncertainties in the range 1.2–2.5% [65–67], while the overall uncertainty for the 2016–2018 period is 1.6%.

Uncertainties in muon identification and trigger efficiencies, as determined using a "tag-and-probe" method [68], are estimated to be 1.5% per muon. The efficiencies of track selection and muon+track isolation are evaluated in a study of $Z \to \tau\tau$ events where one tau lepton decays to a muon while the other decays into an isolated track in a 1-prong decay. This track meets the same selection criteria as in the nominal analysis. In this study, scale factors, accounting for

differences in efficiency between data and simulation, are derived and applied to the simulated samples. The uncertainties in scale factors affect the shape of the signal estimate and alter the overall signal yield by 10–20%.

During the 2016–2017 data-taking periods, a timing shift in the ECAL L1 trigger inputs from the forward endcap region ($|\eta| > 2.4$) caused inefficiencies by incorrectly associating events with the previous bunch crossing [38]. A correction for this effect, determined using an unbiased data sample, is applied to the simulation, accompanied by normalization-altering uncertainties ranging between 0.1 and 2.8%, depending on the a_1 boson mass and signal sample.

The uncertainties in measuring the b tagging efficiency are applied separately to heavy-flavor and light-flavor jets in the simulated samples as described in Ref. [60]. These uncertainties are divided into components specific to the data-taking period and components correlated across periods. The b tagging uncertainties lead to variations in the yield between 0.2 and 0.5%.

Theoretical uncertainties impact the kinematic distributions of the Higgs boson, particularly its p_T spectrum, thereby affecting the signal acceptance. The uncertainty due to missing higher-order corrections in the ggF process is estimated using the HqT program by varying independently the renormalization (μ_R) and factorization (μ_F) scales by factors of 0.5 and 2. The p_T-dependent *K*-factors are recomputed according to these variations and applied to the simulated signal samples. The resulting effect on the signal acceptance varies between 2.5 and 3%, depending on m_{a_1}. Similarly, uncertainties in the signal acceptance for the VBF and VH processes are computed, with impacts ranging from 1 to 3%, according to the process and m_{a_1}.

The HqT program is also used to evaluate the uncertainties arising from the choice of PDFs for the ggF process. Nominal *K*-factors for the p_T spectrum of the Higgs boson are computed using the NNPDF3.1 PDF set [69]. Variations within the uncertainties in the NNPDF3.1 PDFs alter the signal acceptance by approximately 1%. The impact of the PDF uncertainties on the acceptance of the VBF and VH processes is estimated in a similar way, resulting in a 2% uncertainty.

Systematic uncertainties in the theoretical predictions for the Higgs boson production cross section are driven by variations of the μ_F and μ_R scales and the PDF uncertainties. Uncertainties related to scale variations range from 1 to 5%, depending on the Higgs boson production mode, whereas the uncertainties related to PDF vary between 1 and 3%.

Bin-by-bin statistical uncertainties in $C(i, j)$, related to the limited size of the data sample in *CR Loose-Iso*, constitute the dominant uncertainty across all probed mass hypotheses. Additionally, shape uncertainties related to the modeling of $f_{1D}(i)$ have a substantial effect. For higher m_{a_1}, the uncertainty associated with the track selection and muon+track isolation efficiency also becomes significant.

10 Results

The signal is extracted with a binned maximum-likelihood fit applied to the 2D (m_1, m_2) distribution, using the CMS statistical analysis tool COMBINE [70], based on the ROOFIT [71] and ROOSTATS [72] frameworks. The normalizations of both the signal and background are allowed to float freely in the fit. Systematic uncertainties affecting the normalization of the signal templates are incorporated via nuisance parameters with log-normal distributions. Shape-altering systematic uncertainties are modeled by nuisance parameters whose variations cause continuous morphing of the signal or background template shapes, as discussed in Section 4.2.1 of Ref. [70], and are assigned Gaussian prior probability density functions. For each probed m_{a_1},

the (m_1, m_2) distribution is fitted with the sum of five templates: one for the background model and four for the signal. The signal templates correspond to the ggF, VBF, and VH production modes with $H \to a_1 a_1 \to 4\tau$, and the inclusive Higgs boson production followed by $H \to a_1 a_1 \to 2\mu 2\tau$. The normalization of the signal templates is scaled by a common signal strength modifier. The yields of the 4τ and $2\mu 2\tau$ signals are related according to Eqs. (1) and (2). No significant excess of events over the SM background prediction is observed. The compatibility of the observed (m_1, m_2) distribution with the background-only model is quantified with a goodness-of-fit test based on the saturated model for the test statistics [73, 74], yielding a p-value of 0.45.

Figure 8 displays the unrolled (m_1, m_2) distribution, where the notation for the bins follows that of Fig. 2. For illustrative purposes, the background distribution is normalized by fitting the observed data under the background-only hypothesis. Expectations for the signal for m_{a_1} = 5, 8, 12, and 15 GeV are also shown. The signal normalization is calculated assuming the SM prediction for the cross sections of the ggF, VBF, and VH processes and a branching fraction of 5% for the $H \to a_1 a_1 \to 4\tau$ decays.

The results of the analysis are used to set upper limits at 95% CL on the product of the cross section and branching fractions, $\sigma(pp \to H + X)\mathcal{B}(H \to a_1 a_1)\mathcal{B}^2(a_1 \to \tau\tau)$, relative to the inclusive SM Higgs boson production cross section, σ_{SM}. The CL_s criterion [75, 76] is used to set the upper limits, using the asymptotic approximation [77]. The test statistic employed in the statistical inference is the profile likelihood ratio modified for upper limits [78]. Figure 9 shows the obtained observed and expected upper limits. The observed limits vary from 0.007 at $m_{a_1} = 11$ GeV to 0.079 at $m_{a_1} = 4$ GeV. The expected upper limits in the absence of signal range between 0.011 at $m_{a_1} = 11$ GeV to 0.066 at $m_{a_1} = 4$ GeV. The observed upper limits are compatible with the expected limits within two standard deviations over the entire m_{a_1} range.

The (m_1, m_2) distribution shows a deficit in the observed yields with respect to the background-only expectations prior to the fit, primarily along the diagonal and near-diagonal bins. These bins contain the bulk of the $H \to a_1 a_1$ signal events, as expected for the decay of the Higgs boson into two identical bosons. To assess the pre-fit agreement between data and the background model, the background distribution is normalized to the total number of events observed in the *SR*. The most pronounced deviations occur in bins (2,2), (2,3), (4,4), (4,5), and (4,6). This deficit results in observed upper limits that are stronger than the expected across a broad range of m_{a_1}. The largest discrepancy between the observed and expected limits amounts to 1.7 standard deviations, at $m_{a_1} = 8$ GeV. It should be reiterated at this point that the background distribution shown in Fig. 8 is obtained after performing the fit to data under the background-only hypothesis, wherein the differences between the observed and expected yields in individual (m_1, m_2) bins are mitigated by variations of the nuisance parameters included in the statistical model.

The decrease in sensitivity observed at lower m_{a_1} values is caused by the increase in background towards smaller muon+track invariant mass, as illustrated in Figs. 4 and 8. As m_{a_1} increases, the average angular separation between the decay products of the a_1 boson increases. Consequently, the efficiency of the signal selection decreases due to the requirement that the muon and the track from the $a_1 \to \tau_\mu \tau_{1\text{-prong}}$ or $a_1 \to \mu\mu$ decay must be within a cone of $\Delta R = 0.5$. This explains the reduced sensitivity at higher values of m_{a_1}.

The inclusion of the $H \to a_1 a_1 \to 2\mu 2\tau$ channel in the signal model consistently improves both the expected and observed limits across all mass points, with improvements ranging from 25 to 35% in the expected limits and up to 30% in the observed limits. The sizable improvement

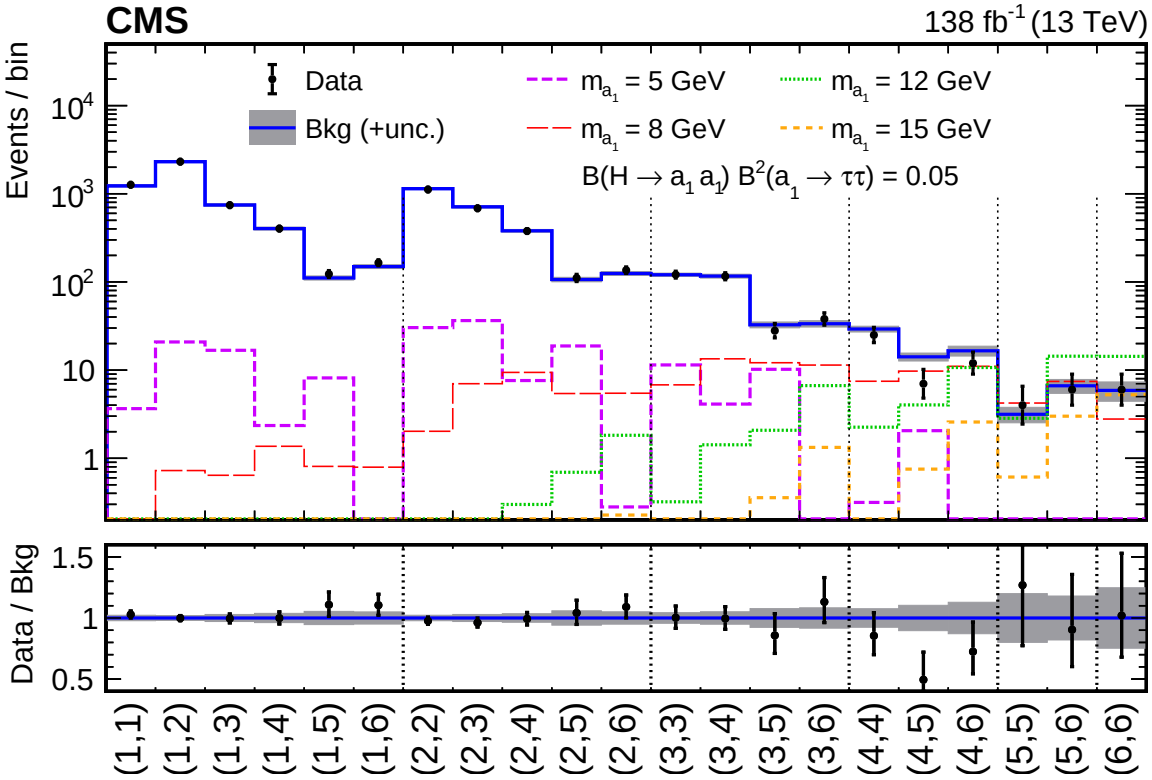

Figure 8: The unrolled (m_1, m_2) distribution used to extract the signal. The observed number of events in data is represented by the points, with the vertical bars giving the statistical uncertainty. The background is shown as the blue histogram, with its uncertainty depicted by the shaded grey band. The normalization for the background is obtained by fitting the observed data under the background-only hypothesis. Signal expectations for the 4τ and $2\mu2\tau$ final states are shown as dashed histograms for the mass hypotheses m_{a_1} = 5, 8, 12, and 15 GeV. The relative normalization of the 4τ and $2\mu2\tau$ final states is given by Eq. (1). The signal normalization is computed assuming that the Higgs boson is produced in pp collisions with a rate predicted by the SM and decays into the $a_1a_1 \to 4\tau$ final state with a branching fraction of 5%. The lower plot shows the ratio of the observed data events to the expected background yield in each bin of the (m_1, m_2) distribution.

of sensitivity with the inclusion of the $2\mu2\tau$ channel is driven by two factors. Firstly, $\mathcal{A}\epsilon$ for the $2\mu2\tau$ channel is higher compared to that for 4τ because of the substantially harder p_T spectrum of muons in $a_1 \to \mu\mu$ decays than in $a_1 \to \tau_\mu\tau_{1\text{-prong}}$ decays. Secondly, the $a_1 \to \mu\mu$ decay produces resonant structures in the m_1 distribution, making the discrimination between signal and background in the $2\mu2\tau$ channel more efficient than in the 4τ channel.

The results of the search are also interpreted in the context of the 2HD+S models. The upper limits on the signal strength are translated into constraints on $\sigma(pp \to H + X)\mathcal{B}(H \to a_1a_1)$ by scaling them with the theoretically predicted values of $\mathcal{B}^2(a_1 \to \tau\tau)$. The branching fraction, which depends on the model type, m_{a_1}, and $\tan\beta$, is calculated using the decay width expressions from Ref. [79]. Figure 10 shows the observed and expected 95% CL upper limits on $\sigma(pp \to H + X)\mathcal{B}(H \to a_1a_1)$ obtained for the four types of 2HD+S models at benchmark values of $\tan\beta$, corresponding to scenarios where the $a_1 \to \tau\tau$ decay has a sizable branching fraction. Among the scenarios considered, the Type III 2HD+S model with $\tan\beta = 2$ provides the most stringent limits across all m_{a_1} values between 4 and 15 GeV. The observed upper lim-

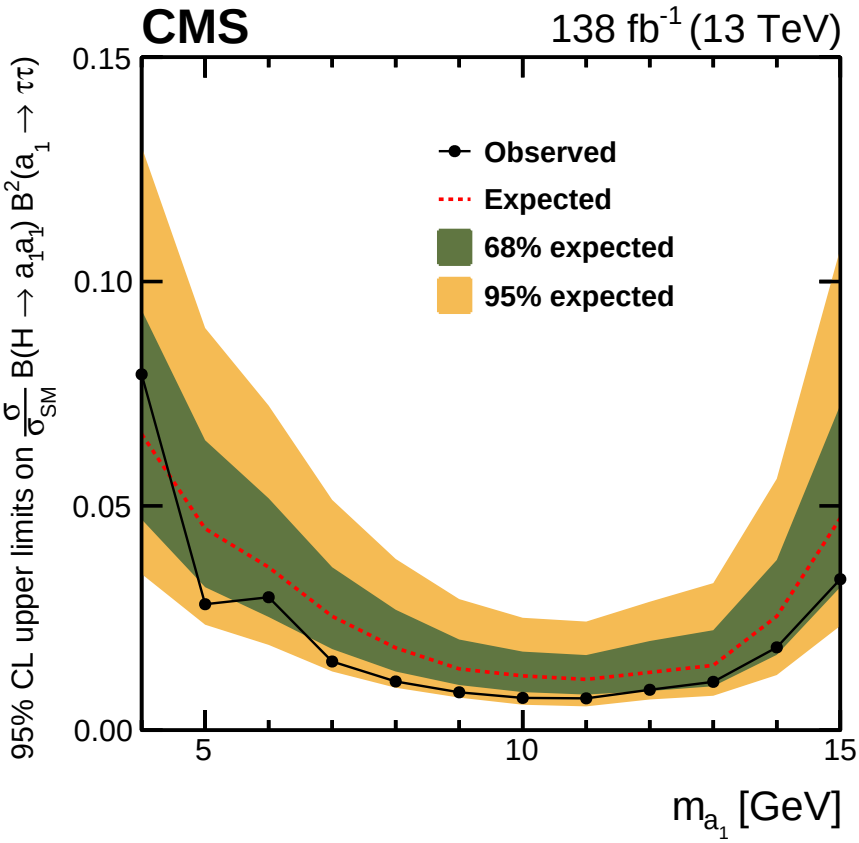

Figure 9: The observed (points) and expected (red line) 95% CL upper limits on the product of the signal cross section and the branching fractions $\sigma(\mathrm{pp} \to \mathrm{H} + \mathrm{X})\mathcal{B}(\mathrm{H} \to \mathrm{a_1 a_1})\mathcal{B}^2(\mathrm{a_1} \to \tau\tau)$, relative to the inclusive Higgs boson production cross section σ_{SM} predicted in the SM. The green and yellow bands indicate the regions containing 68 and 95% of the expected limit ranges under the background-only hypothesis.

its range from 0.010 at $m_{\mathrm{a_1}} = 9\,\mathrm{GeV}$ to 0.35 at $m_{\mathrm{a_1}} = 4\,\mathrm{GeV}$. For the Type II model, for $\tan\beta = 5$, tight constraints between 0.013 and 0.092 are obtained for $m_{\mathrm{a_1}}$ up to 9 GeV. Above 9 GeV, the decay of $\mathrm{a_1}$ to bottom quarks overwhelms the decay to tau leptons, making the analysis less sensitive. In the Type I 2HD+S model, $\mathrm{a_1}$ couplings to fermions are independent of $\tan\beta$, so the upper limit depends only on $m_{\mathrm{a_1}}$. The branching fraction to $\tau\tau$ is less enhanced since it has to compete with other decays, such as those to charm and bottom quark pairs. Thus, the analysis yields less stringent constraints on $\sigma(\mathrm{pp} \to \mathrm{H} + \mathrm{X})\mathcal{B}(\mathrm{H} \to \mathrm{a_1 a_1})$, ranging from 0.038 at 9 GeV to 29 at 4 GeV. For the Type IV model, the analysis is only sensitive for $\tan\beta < 1$, since at higher values the decays to quarks dominate in the considered mass range. At $\tan\beta = 0.5$, the analysis sets observed upper limits between 0.039 at 9 GeV and 29 at 4 GeV.

The peak-like structures seen in the expected limits of Fig. 10 occur in $m_{\mathrm{a_1}}$ regions where quarkonium states, such as η_{c} and η_{b}, are found. In these regions, the mixing of $\mathrm{a_1}$-quarkonium states plays a crucial role, leading to a sudden increase in the hadronic decay width due to nonperturbative QCD effects. This results in a significant decrease of the branching fractions to unbound systems, such as $\tau\tau$. The mixing of $\mathrm{a_1}$ with η_c (η_b) is significantly amplified in scenarios where the coupling of $\mathrm{a_1}$ to charm (bottom) quarks is enhanced. Further details of the $\mathrm{a_1}$-quarkonium mixing can be found in Refs. [79, 80]. As a result of the mixing, the analysis fails to provide tight constraints in these mass regions.

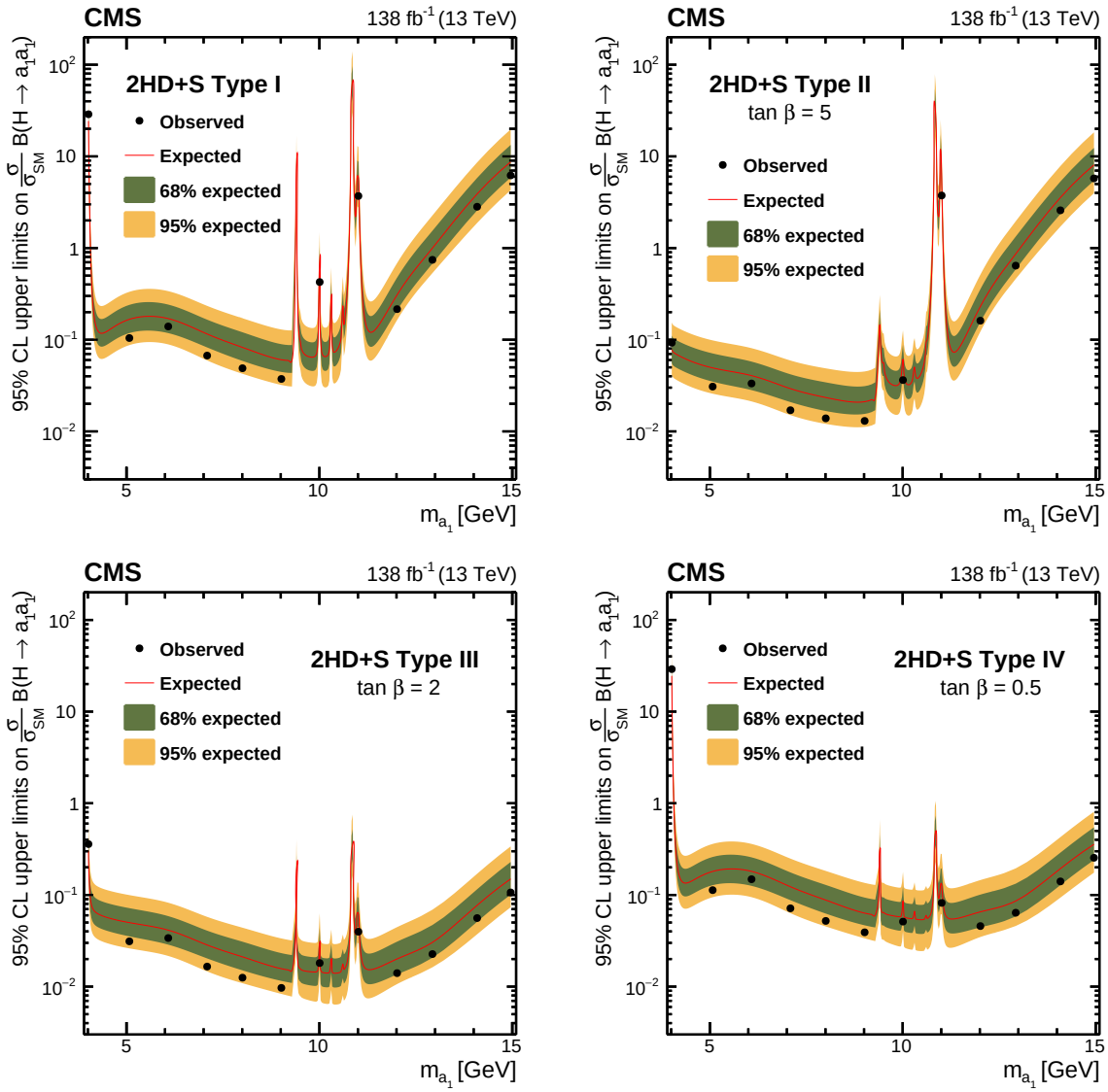

Figure 10: The observed (points) and expected (red line) 95% CL upper limits on $\sigma(\mathrm{pp} \to \mathrm{H} + \mathrm{X})\mathcal{B}(\mathrm{H} \to \mathrm{a_1 a_1})$, relative to σ_{SM}, as a function of $m_{\mathrm{a_1}}$ for different 2HD+S models at benchmark $\tan\beta$ values: Type I ($\tan\beta$ independent; upper left), Type II ($\tan\beta = 5$; upper right), Type III ($\tan\beta = 2$; lower left), and Type IV ($\tan\beta = 0.5$; lower right).

Upper limits at 95% CL are also set on $\sigma(\mathrm{pp} \to \mathrm{H} + \mathrm{X})\mathcal{B}(\mathrm{H} \to \mathrm{a_1 a_1})$, relative to σ_{SM}, as a function of $\tan\beta$ for benchmark $\mathrm{a_1}$ boson masses. Figures 11 and 12 present the limits obtained for Type II and Type III 2HD+S models, respectively, for $m_{\mathrm{a_1}} = 5$, 8, 12, and 15 GeV. For both models, the analysis sets stringent constraints for $\tan\beta > 1$, where the coupling to tau leptons is enhanced. For $\tan\beta < 1$, decays of the $\mathrm{a_1}$ boson to quarks dominate and suppress the $\tau\tau$ decay, resulting in weaker limits. The Type III 2HD+S model provides the best constraints for $\tan\beta > 1$ across all considered $m_{\mathrm{a_1}}$ values. In the Type II model, tight constraints are obtained for $5 < m_{\mathrm{a_1}} < 8$ GeV, but the limits deteriorate for higher masses due to the enhanced Yukawa coupling to b quarks. The observed deterioration of the limits at lower and higher $\mathrm{a_1}$ masses for both models can be directly related to the trends observed in the model-independent results. The enhanced b quark coupling plays an additional role in weakening the limits for higher masses in the Type II model.

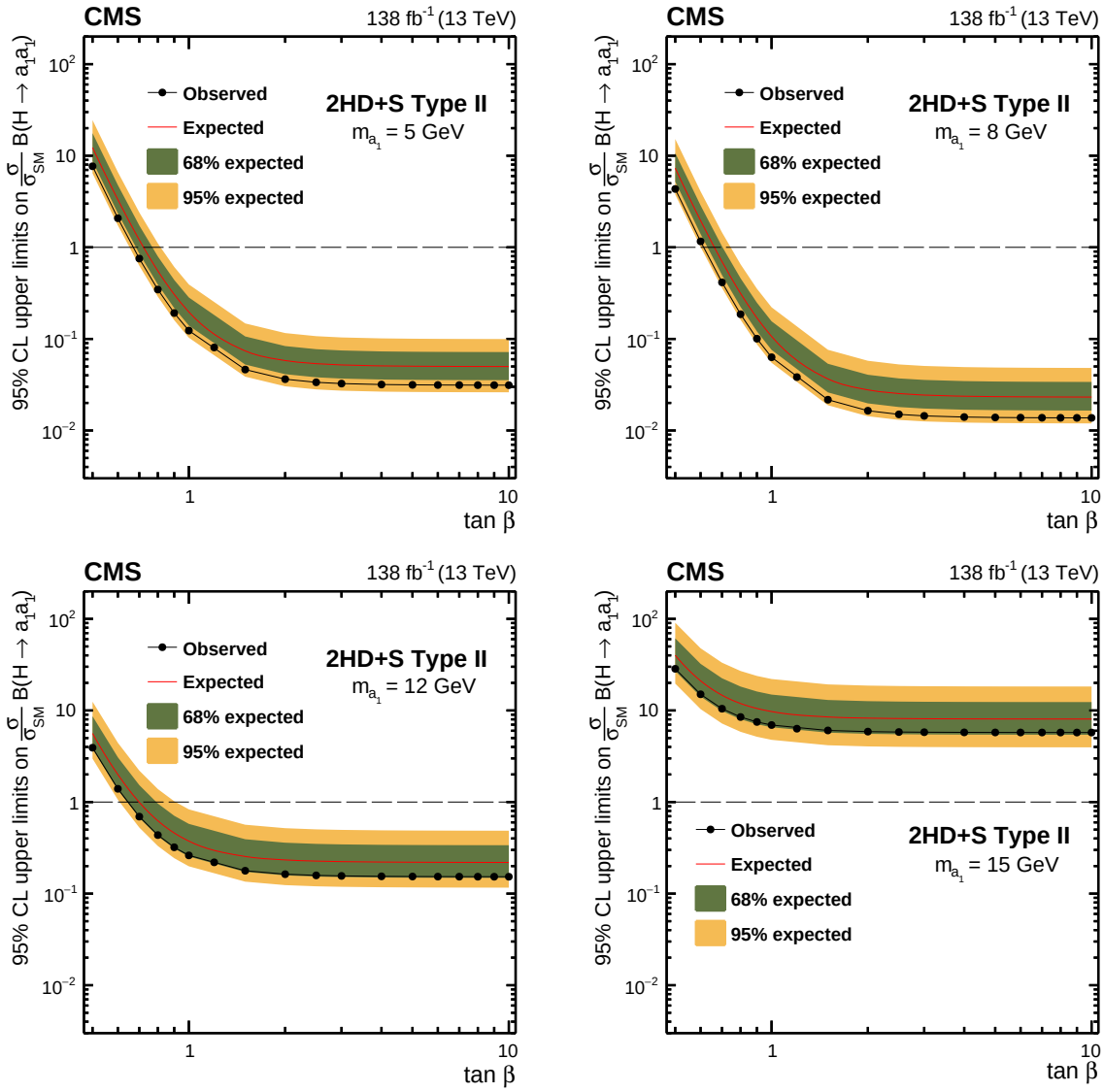

Figure 11: The observed (points) and expected (red line) 95% CL upper limits on $\sigma(\mathrm{pp} \to \mathrm{H} + \mathrm{X})\mathcal{B}(\mathrm{H} \to \mathrm{a}_1\mathrm{a}_1)$, relative to σ_{SM}, as a function of $\tan\beta$ for the Type II 2HD+S model with $m_{\mathrm{a}_1} = 5\,\mathrm{GeV}$ (upper left), $m_{\mathrm{a}_1} = 8\,\mathrm{GeV}$ (upper right), $m_{\mathrm{a}_1} = 12\,\mathrm{GeV}$ (lower left), and $m_{\mathrm{a}_1} = 15\,\mathrm{GeV}$ (lower right).

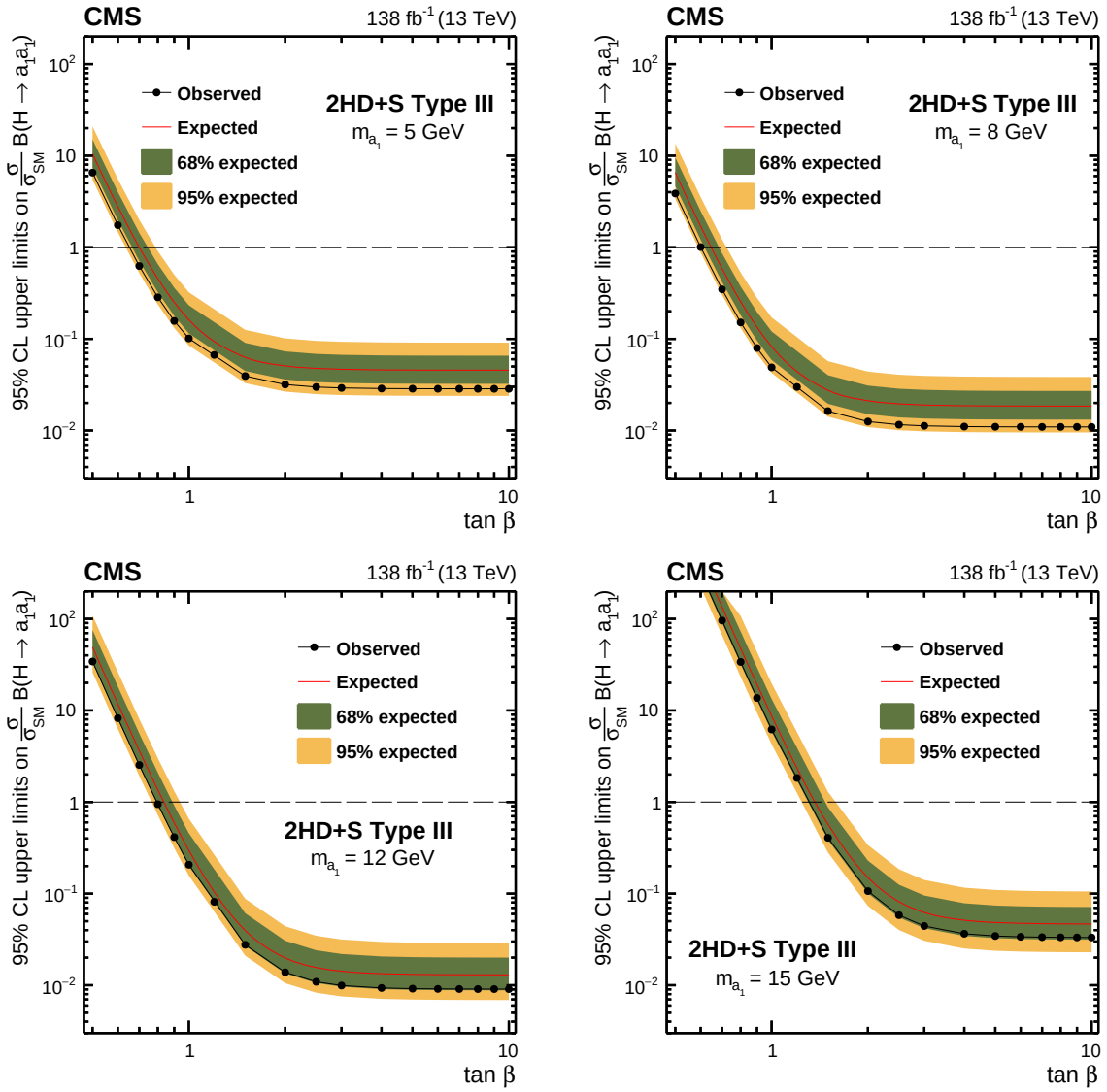

Figure 12: The observed (points) and expected (red line) 95% CL upper limits on $\sigma(\mathrm{pp} \to \mathrm{H} + \mathrm{X})\mathcal{B}(\mathrm{H} \to \mathrm{a}_1\mathrm{a}_1)$, relative to σ_{SM}, as a function of $\tan\beta$ for the Type III 2HD+S model with $m_{\mathrm{a}_1} = 5\,\mathrm{GeV}$ (upper left), $m_{\mathrm{a}_1} = 8\,\mathrm{GeV}$ (upper right), $m_{\mathrm{a}_1} = 12\,\mathrm{GeV}$ (lower left), and $m_{\mathrm{a}_1} = 15\,\mathrm{GeV}$ (lower right).

11 Summary

A search for a pair of light pseudoscalar bosons (a_1) produced in decays of the 125 GeV Higgs boson (H), $H \to a_1 a_1$, in final states with two muons and two charged-particle tracks is presented. The search is performed using data from proton-proton collisions at a center-of-mass energy of 13 TeV, collected by the CMS experiment at the LHC between 2016 and 2018, and corresponding to an integrated luminosity of 138 fb^{-1}. The analysis exploits the gluon-gluon fusion, vector boson fusion, and Higgs-strahlung production modes, and targets the $H \to a_1 a_1 \to 4\tau$ and $2\mu 2\tau$ decay channels. Masses of the a_1 boson (m_{a_1}) in the range 4–15 GeV are examined. No excess of data above the standard model (SM) background prediction is found. Upper limits on the product of the inclusive signal cross section and the branching fraction, $\sigma(pp \to H + X)\mathcal{B}(H \to a_1 a_1)\mathcal{B}^2(a_1 \to \tau\tau)$, relative to the SM Higgs boson production cross section σ_{SM}, are set at 95% confidence level (CL) by combining the 4τ and $2\mu 2\tau$ decay channels, assuming Yukawa-like couplings of a_1 to fermions. The observed limits range from 0.007 at $m_{a_1} = 11$ GeV to 0.079 at $m_{a_1} = 4$ GeV. The expected limits in the absence of signal span from 0.011 at $m_{a_1} = 11$ GeV to 0.066 at $m_{a_1} = 4$ GeV. The results are a significant improvement over the previous CMS analysis at 13 TeV [29], exceeding the anticipated improvement from the larger data sample alone. The sensitivity is enhanced by a factor of 2 to 4, depending on m_{a_1}, which can be attributed to the introduction of a veto for b-tagged jets and further optimization of the selection criteria targeting the $a_1 \to \tau\tau$ and $\mu\mu$ decays. The analysis also exceeds the sensitivity of a similar search performed by the ATLAS Collaboration in the same channel using a comparable amount of integrated luminosity [33].

The results of the search are also interpreted in the context of various models with two Higgs doublets and an additional complex singlet field (2HD+S). For the Type II 2HD+S scenario, realized in the next-to-minimal supersymmetric SM, 95% CL upper limits between 0.013 and 0.092 are set on $\sigma(pp \to H + X)\mathcal{B}(H \to a_1 a_1)$, relative to σ_{SM}, for $4 < m_{a_1} < 9$ GeV and $\tan\beta > 5$. The analysis sets the most stringent constraints to date for the Type III 2HD+S scenario. Upper limits in the range 0.010–0.057 are obtained for probed mass hypotheses in the ranges $5 < m_{a_1} < 9$ GeV and $12 < m_{a_1} < 14$ GeV for $\tan\beta > 2$.

Acknowledgments

We congratulate our colleagues in the CERN accelerator departments for the excellent performance of the LHC and thank the technical and administrative staffs at CERN and at other CMS institutes for their contributions to the success of the CMS effort. In addition, we gratefully acknowledge the computing centers and personnel of the Worldwide LHC Computing Grid and other centers for delivering so effectively the computing infrastructure essential to our analyses. Finally, we acknowledge the enduring support for the construction and operation of the LHC, the CMS detector, and the supporting computing infrastructure provided by the following funding agencies: SC (Armenia), BMBWF and FWF (Austria); FNRS and FWO (Belgium); CNPq, CAPES, FAPERJ, FAPERGS, and FAPESP (Brazil); MES and BNSF (Bulgaria); CERN; CAS, MoST, and NSFC (China); MINCIENCIAS (Colombia); MSES and CSF (Croatia); RIF (Cyprus); SENESCYT (Ecuador); ERC PRG, TARISTU24-TK10 and MoER TK202 (Estonia); Academy of Finland, MEC, and HIP (Finland); CEA and CNRS/IN2P3 (France); SRNSF (Georgia); BMBF, DFG, and HGF (Germany); GSRI (Greece); NKFIH (Hungary); DAE and DST (India); IPM (Iran); SFI (Ireland); INFN (Italy); MSIT and NRF (Republic of Korea); MES (Latvia); LMTLT (Lithuania); MOE and UM (Malaysia); BUAP, CINVESTAV, CONACYT, LNS, SEP, and UASLP-FAI (Mexico); MOS (Montenegro); MBIE (New Zealand); PAEC (Pakistan); MES and

NSC (Poland); FCT (Portugal); MESTD (Serbia); MICIU/AEI and PCTI (Spain); MOSTR (Sri Lanka); Swiss Funding Agencies (Switzerland); MST (Taipei); MHESI and NSTDA (Thailand); TUBITAK and TENMAK (Türkiye); NASU (Ukraine); STFC (United Kingdom); DOE and NSF (USA).

Individuals have received support from the Marie-Curie program and the European Research Council and Horizon 2020 Grant, contract Nos. 675440, 724704, 752730, 758316, 765710, 824093, 101115353, 101002207, 101001205, and COST Action CA16108 (European Union); the Leventis Foundation; the Alfred P. Sloan Foundation; the Alexander von Humboldt Foundation; the Science Committee, project no. 22rl-037 (Armenia); the Fonds pour la Formation à la Recherche dans l'Industrie et dans l'Agriculture (FRIA-Belgium); the Beijing Municipal Science & Technology Commission, No. Z191100007219010, the Fundamental Research Funds for the Central Universities, the Ministry of Science and Technology of China under Grant No. 2023YFA1605804, and the Natural Science Foundation of China under Grant No. 12061141002 (China); the Ministry of Education, Youth and Sports (MEYS) of the Czech Republic; the Shota Rustaveli National Science Foundation, grant FR-22-985 (Georgia); the Deutsche Forschungsgemeinschaft (DFG), among others, under Germany's Excellence Strategy – EXC 2121 "Quantum Universe" – 390833306, and under project number 400140256 - GRK2497; the Hellenic Foundation for Research and Innovation (HFRI), Project Number 2288 (Greece); the Hungarian Academy of Sciences, the New National Excellence Program - ÚNKP, the NKFIH research grants K 131991, K 133046, K 138136, K 143460, K 143477, K 146913, K 146914, K 147048, 2020-2.2.1-ED-2021-00181, TKP2021-NKTA-64, and 2021-4.1.2-NEMZ_KI-2024-00036 (Hungary); the Council of Science and Industrial Research, India; ICSC – National Research Center for High Performance Computing, Big Data and Quantum Computing, FAIR – Future Artificial Intelligence Research, and CUP I53D23001070006 (Mission 4 Component 1), funded by the NextGenerationEU program (Italy); the Latvian Council of Science; the Ministry of Education and Science, project no. 2022/WK/14, and the National Science Center, contracts Opus 2021/41/B/ST2/01369 and 2021/43/B/ST2/01552 (Poland); the Fundação para a Ciência e a Tecnologia, grant CEECIND/01334/2018 (Portugal); the National Priorities Research Program by Qatar National Research Fund; MICIU/AEI/10.13039/501100011033, ERDF/EU, "European Union NextGenerationEU/PRTR", and Programa Severo Ochoa del Principado de Asturias (Spain); the Chulalongkorn Academic into Its 2nd Century Project Advancement Project, and the National Science, Research and Innovation Fund via the Program Management Unit for Human Resources & Institutional Development, Research and Innovation, grant B39G680009 (Thailand); the Kavli Foundation; the Nvidia Corporation; the SuperMicro Corporation; the Welch Foundation, contract C-1845; and the Weston Havens Foundation (USA).

References

[1] ATLAS Collaboration, "Observation of a new particle in the search for the standard model Higgs boson with the ATLAS detector at the LHC", *Phys. Lett. B* **716** (2012) 1, doi:10.1016/j.physletb.2012.08.020, arXiv:1207.7214.

[2] CMS Collaboration, "Observation of a new boson at a mass of 125 GeV with the CMS experiment at the LHC", *Phys. Lett. B* **716** (2012) 30, doi:10.1016/j.physletb.2012.08.021, arXiv:1207.7235.

[3] CMS Collaboration, "Observation of a new boson with mass near 125 GeV in pp collisions at $\sqrt{s} = 7$ and 8 TeV", *JHEP* **06** (2013) 081, doi:10.1007/JHEP06(2013)081, arXiv:1303.4571.

[4] ATLAS Collaboration, "A detailed map of Higgs boson interactions by the ATLAS experiment ten years after the discovery", *Nature* **607** (2022) 52, doi:10.1038/s41586-022-04893-w, arXiv:2207.00092. [Erratum: doi:doi:10.1016/0370-2693(84)91890-2].

[5] CMS Collaboration, "A portrait of the Higgs boson by the CMS experiment ten years after the discovery.", *Nature* **607** (2022) 60, doi:10.1038/s41586-022-04892-x, arXiv:2207.00043. [Author correction: doi:doi:10.1038/s41586-023-06164-8].

[6] T. D. Lee, "A theory of spontaneous T violation", *Phys. Rev. D* **8** (1973) 1226, doi:10.1103/PhysRevD.8.1226.

[7] G. C. Branco et al., "Theory and phenomenology of two-Higgs-doublet models", *Phys. Rept.* **516** (2012) 1, doi:10.1016/j.physrep.2012.02.002, arXiv:1106.0034.

[8] D. Curtin et al., "Exotic decays of the 125 GeV Higgs boson", *Phys. Rev. D* **90** (2014) 075004, doi:10.1103/PhysRevD.90.075004, arXiv:1312.4992.

[9] P. Fayet, "Supergauge invariant extension of the Higgs mechanism and a model for the electron and its neutrino", *Nucl. Phys. B* **90** (1975) 104, doi:10.1016/0550-3213(75)90636-7.

[10] P. Fayet, "Spontaneously broken supersymmetric theories of weak, electromagnetic and strong interactions", *Phys. Lett. B* **69** (1977) 489, doi:10.1016/0370-2693(77)90852-8.

[11] U. Ellwanger, C. Hugonie, and A. M. Teixeira, "The next-to-minimal supersymmetric standard model", *Phys. Rept.* **496** (2010) 1, doi:10.1016/j.physrep.2010.07.001, arXiv:0910.1785.

[12] M. Maniatis, "The next-to-minimal supersymmetric extension of the standard model reviewed", *Int. J. Mod. Phys. A* **25** (2010) 3505, doi:10.1142/S0217751X10049827, arXiv:0906.0777.

[13] J. E. Kim and H. P. Nilles, "The μ-problem and the strong CP-problem", *Phys. Lett. B* **138** (1984) 150, doi:10.1016/0370-2693(84)91890-2.

[14] S. Ramos-Sanchez, "The μ-problem, the NMSSM and string theory", *Fortsch. Phys.* **58** (2010) 748, doi:10.1002/prop.201000058, arXiv:1003.1307.

[15] ATLAS Collaboration, "Search for new light gauge bosons in Higgs boson decays to four-lepton final states in pp collisions at $\sqrt{s}$ = 8 TeV with the ATLAS detector at the LHC", *Phys. Rev. D* **92** (2015) 092001, doi:10.1103/PhysRevD.92.092001, arXiv:1505.07645.

[16] CMS Collaboration, "Search for a non-standard-model Higgs boson decaying to a pair of new light bosons in four-muon Final States", *Phys. Lett. B* **726** (2013) 564, doi:10.1016/j.physletb.2013.09.009, arXiv:1210.7619.

[17] CMS Collaboration, "A search for pair production of new light bosons decaying into muons", *Phys. Lett. B* **752** (2016) 146, doi:10.1016/j.physletb.2015.10.067, arXiv:1506.00424.

[18] CMS Collaboration, "Search for light bosons in decays of the 125 GeV Higgs boson in proton-proton collisions at $\sqrt{s}$ = 8 TeV", *JHEP* **10** (2017) 076, doi:10.1007/JHEP10(2017)076, arXiv:1701.02032.

[19] CMS Collaboration, "Search for a very light NMSSM Higgs boson produced in decays of the 125 GeV scalar boson and decaying into τ leptons in pp collisions at $\sqrt{s}$ = 8 TeV", *JHEP* **01** (2016) 079, doi:10.1007/JHEP01(2016)079, arXiv:1510.06534.

[20] ATLAS Collaboration, "Search for new phenomena in events with at least three photons collected in pp collisions at $\sqrt{s}$ = 8 TeV with the ATLAS detector", *Eur. Phys. J. C* **76** (2016) 210, doi:10.1140/epjc/s10052-016-4034-8, arXiv:1509.05051.

[21] ATLAS Collaboration, "Search for Higgs boson decays to beyond-the-standard-model light bosons in four-lepton events with the ATLAS detector at $\sqrt{s}$ = 13 TeV", *JHEP* **06** (2018) 166, doi:10.1007/JHEP06(2018)166, arXiv:1802.03388.

[22] CMS Collaboration, "A search for pair production of new light bosons decaying into muons in proton-proton collisions at 13 TeV", *Phys. Lett. B* **796** (2019) 131, doi:10.1016/j.physletb.2019.07.013, arXiv:1812.00380.

[23] ATLAS Collaboration, "Search for Higgs bosons decaying to aa in the $\mu\mu\tau\tau$ final state in pp collisions at $\sqrt{s}$ = 8 TeV with the ATLAS experiment", *Phys. Rev. D* **92** (2015) 052002, doi:10.1103/PhysRevD.92.052002, arXiv:1505.01609.

[24] CMS Collaboration, "Search for an exotic decay of the Higgs boson to a pair of light pseudoscalars in the final state of two muons and two τ leptons in proton-proton collisions at $\sqrt{s}$ = 13 TeV", *JHEP* **11** (2018) 018, doi:10.1007/JHEP11(2018)018, arXiv:1805.04865.

[25] CMS Collaboration, "Search for a light pseudoscalar Higgs boson in the boosted $\mu\mu\tau\tau$ final state in proton-proton collisions at $\sqrt{s}$ = 13 TeV", *JHEP* **08** (2020) 139, doi:10.1007/JHEP08(2020)139, arXiv:2005.08694.

[26] ATLAS Collaboration, "Search for Higgs boson decays into a pair of light bosons in the bb$\mu\mu$ final state in pp collision at $\sqrt{s}$ = 13 TeV with the ATLAS detector", *Phys. Lett. B* **790** (2019) 1, doi:10.1016/j.physletb.2018.10.073, arXiv:1807.00539.

[27] CMS Collaboration, "Search for exotic decays of the Higgs boson to a pair of pseudoscalars in the $\mu\mu$bb and $\tau\tau$bb final states", *Eur. Phys. J. C* **84** (2024) 493, doi:10.1140/epjc/s10052-024-12727-4, arXiv:2402.13358.

[28] ATLAS Collaboration, "Search for Higgs boson decays into pairs of light (pseudo)scalar particles in the $\gamma\gamma$jj final state in pp collisions at $\sqrt{s}$ = 13 TeV with the ATLAS detector", *Phys. Lett. B* **782** (2018) 750, doi:10.1016/j.physletb.2018.06.011, arXiv:1803.11145.

[29] CMS Collaboration, "Search for light pseudoscalar boson pairs produced from decays of the 125 GeV Higgs boson in final states with two muons and two nearby tracks in pp collisions at $\sqrt{s}$ = 13 TeV", *Phys. Lett. B* **800** (2020) 135087, doi:10.1016/j.physletb.2019.135087, arXiv:1907.07235.

[30] CMS Collaboration, "Search for the decay of the Higgs boson to a pair of light pseudoscalar bosons in the final state with four bottom quarks in proton-proton collisions at $\sqrt{s}$ = 13 TeV", *JHEP* **06** (2024) 097, doi:10.1007/JHEP06(2024)097, arXiv:2403.10341.

[31] CMS Collaboration, "Search for the exotic decay of the Higgs boson into two light pseudoscalars with four photons in the final state in proton-proton collisions at $\sqrt{s} = 13$ TeV", *JHEP* **07** (2023) 148, doi:10.1007/JHEP07(2023)148, arXiv:2208.01469.

[32] CMS Collaboration, "Search for exotic Higgs boson decays $H \to \mathcal{A}\mathcal{A} \to 4\gamma$ with events containing two merged diphotons in proton-proton collisions at $\sqrt{s} = 13$ TeV", *Phys. Rev. Lett.* **131** (2023) 101801, doi:10.1103/PhysRevLett.131.101801, arXiv:2209.06197.

[33] ATLAS Collaboration, "Search for Higgs boson exotic decays into Lorentz-boosted light bosons in the four-τ final state at $\sqrt{s} = 13$ TeV with the ATLAS detector", 2025. arXiv:2503.05463. Submitted to *Phys. Lett. B*.

[34] CMS Collaboration, "Identification of hadronic tau lepton decays using a deep neural network", *JINST* **17** (2022) P07023, doi:10.1088/1748-0221/17/07/P07023, arXiv:2201.08458.

[35] HEPData record for this analysis, 2025. doi:10.17182/hepdata.158360.

[36] CMS Collaboration, "The CMS experiment at the CERN LHC", *JINST* **3** (2008) S08004, doi:10.1088/1748-0221/3/08/S08004.

[37] CMS Collaboration, "Development of the CMS detector for the CERN LHC Run 3", *JINST* **19** (2024) P05064, doi:10.1088/1748-0221/19/05/P05064, arXiv:2309.05466.

[38] CMS Collaboration, "Performance of the CMS Level-1 trigger in proton-proton collisions at $\sqrt{s} = 13$ TeV", *JINST* **15** (2020) P10017, doi:10.1088/1748-0221/15/10/P10017, arXiv:2006.10165.

[39] CMS Collaboration, "The CMS trigger system", *JINST* **12** (2017) P01020, doi:10.1088/1748-0221/12/01/P01020, arXiv:1609.02366.

[40] CMS Collaboration, "Performance of the CMS high-level trigger during LHC Run 2", *JINST* **19** (2024) P11021, doi:10.1088/1748-0221/19/11/P11021, arXiv:2410.17038.

[41] T. Sjöstrand et al., "An introduction to PYTHIA 8.2", *Comput. Phys. Commun.* **191** (2015) 159, doi:10.1016/j.cpc.2015.01.024, arXiv:1410.3012.

[42] J. Alwall et al., "The automated computation of tree-level and next-to-leading order differential cross sections, and their matching to parton shower simulations", *JHEP* **07** (2014) 079, doi:10.1007/JHEP07(2014)079, arXiv:1405.0301.

[43] G. Bozzi, S. Catani, D. de Florian, and M. Grazzini, "Transverse-momentum resummation and the spectrum of the Higgs boson at the LHC", *Nucl. Phys. B* **737** (2006) 73, doi:10.1016/j.nuclphysb.2005.12.022, arXiv:hep-ph/0508068.

[44] D. de Florian, G. Ferrera, M. Grazzini, and D. Tommasini, "Transverse-momentum resummation: Higgs boson production at the Tevatron and the LHC", *JHEP* **11** (2011) 064, doi:10.1007/JHEP11(2011)064, arXiv:1109.2109.

[45] S. Alioli, P. Nason, C. Oleari, and E. Re, "NLO Higgs boson production via gluon fusion matched with shower in POWHEG", *JHEP* **04** (2009) 002, doi:10.1088/1126-6708/2009/04/002, arXiv:0812.0578.

[46] P. Nason, "A new method for combining NLO QCD with shower Monte Carlo algorithms", *JHEP* **11** (2004) 040, doi:10.1088/1126-6708/2004/11/040, arXiv:hep-ph/0409146.

[47] S. Frixione, P. Nason, and C. Oleari, "Matching NLO QCD computations with parton shower simulations: the POWHEG method", *JHEP* **11** (2007) 070, doi:10.1088/1126-6708/2007/11/070, arXiv:0709.2092.

[48] CMS Collaboration, "Extraction and validation of a new set of CMS PYTHIA8 tunes from underlying-event measurements", *Eur. Phys. J. C* **80** (2020) 4, doi:10.1140/epjc/s10052-019-7499-4, arXiv:1903.12179.

[49] J. Alwall et al., "Comparative study of various algorithms for the merging of parton showers and matrix elements in hadronic collisions", *Eur. Phys. J. C* **53** (2008) 473, doi:10.1140/epjc/s10052-007-0490-5, arXiv:0706.2569.

[50] GEANT4 Collaboration, "GEANT4—a simulation toolkit", *Nucl. Instrum. Meth. A* **506** (2003) 250, doi:10.1016/S0168-9002(03)01368-8.

[51] J. Allison et al., "GEANT4 developments and applications", *IEEE Trans. Nucl. Sci.* **53** (2006) 270, doi:10.1109/TNS.2006.869826.

[52] CMS Collaboration, "Description and performance of track and primary-vertex reconstruction with the CMS tracker", *JINST* **9** (2014) P10009, doi:10.1088/1748-0221/9/10/P10009, arXiv:1405.6569.

[53] CMS Collaboration, "Technical proposal for the Phase-II upgrade of the Compact Muon Solenoid", CMS Technical Proposal CERN-LHCC-2015-010, CMS-TDR-15-02, 2015.

[54] CMS Collaboration, "Particle-flow reconstruction and global event description with the CMS detector", *JINST* **12** (2017) P10003, doi:10.1088/1748-0221/12/10/P10003, arXiv:1706.04965.

[55] CMS Collaboration, "Performance of the CMS muon detector and muon reconstruction with proton-proton collisions at $\sqrt{s}$ = 13 TeV", *JINST* **13** (2018) P06015, doi:10.1088/1748-0221/13/06/P06015, arXiv:1804.04528.

[56] M. Cacciari, G. P. Salam, and G. Soyez, "The anti-k_{T} jet clustering algorithm", *JHEP* **04** (2008) 063, doi:10.1088/1126-6708/2008/04/063, arXiv:0802.1189.

[57] M. Cacciari, G. P. Salam, and G. Soyez, "FastJet user manual", *Eur. Phys. J. C* **72** (2012) 1896, doi:10.1140/epjc/s10052-012-1896-2, arXiv:1111.6097.

[58] CMS Collaboration, "Jet energy scale and resolution in the CMS experiment in pp collisions at 8 TeV", *JINST* **12** (2017) P02014, doi:10.1088/1748-0221/12/02/P02014, arXiv:1607.03663.

[59] E. Bols et al., "Jet Flavour Classification Using DeepJet", *JINST* **15** (2020) P12012, doi:10.1088/1748-0221/15/12/P12012, arXiv:2008.10519.

[60] CMS Collaboration, "Performance summary of AK4 jet b tagging with data from proton-proton collisions at 13 TeV with the CMS detector", CMS Detector Performance Summary CMS-DP-2023-005, 2023.

[61] CMS Collaboration, "Identification of heavy-flavour jets with the CMS detector in pp collisions at 13 TeV", *JINST* **13** (2018) P05011, doi:10.1088/1748-0221/13/05/P05011, arXiv:1712.07158.

[62] LHC Higgs Cross Section Working Group, "Handbook of LHC Higgs cross sections: 4. Deciphering the nature of the Higgs sector", CERN Report CERN-2017-002-M, 2017. doi:10.23731/CYRM-2017-002, arXiv:1610.07922.

[63] M. Lisanti and J. G. Wacker, "Discovering the Higgs boson with low mass muon pairs", *Phys. Rev. D* **79** (2010) 115006, doi:10.1103/PhysRevD.79.115006, arXiv:0903.1377.

[64] R. J. Barlow and C. Beeston, "Fitting using finite Monte Carlo samples", *Comput. Phys. Commun.* **77** (1993) 219, doi:10.1016/0010-4655(93)90005-W.

[65] CMS Collaboration, "Precision luminosity measurement in proton-proton collisions at $\sqrt{s}$ = 13 TeV in 2015 and 2016 at CMS", *Eur. Phys. J. C* **81** (2021) 800, doi:10.1140/epjc/s10052-021-09538-2, arXiv:2104.01927.

[66] CMS Collaboration, "CMS luminosity measurement for the 2017 data-taking period at $\sqrt{s}$ = 13 TeV", CMS Physics Analysis Summary CMS-PAS-LUM-17-004, 2018.

[67] CMS Collaboration, "CMS luminosity measurement for the 2018 data-taking period at $\sqrt{s}$ = 13 TeV", CMS Physics Analysis Summary CMS-PAS-LUM-18-002, 2019.

[68] CMS Collaboration, "Measurement of the inclusive W and Z production cross sections in pp collisions at $\sqrt{s}$ = 7 TeV", *JHEP* **10** (2011) 132, doi:10.1007/JHEP10(2011)132, arXiv:1107.4789.

[69] NNPDF Collaboration, "Parton distributions for the LHC Run II", *JHEP* **04** (2015) 040, doi:10.1007/JHEP04(2015)040, arXiv:1410.8849.

[70] CMS Collaboration, "The CMS statistical analysis and combination tool: Combine", *Comput. Softw. Big Sci.* **8** (2024) 19, doi:10.1007/s41781-024-00121-4, arXiv:2404.06614.

[71] W. Verkerke and D. P. Kirkby, "The RooFit toolkit for data modeling", in *Statistical Problems in Particle Physics, Astrophysics and Cosmology (PHYSTAT 05): Proceedings*, p. 186. 2003. arXiv:physics/0306116. eConf. doi:10.1142/9781860948985_0039.

[72] L. Moneta et al., "The RooStats Project", *PoS* **ACAT2010** (2010) 057, doi:10.22323/1.093.0057, arXiv:1009.1003.

[73] J. K. Lindsey, "Parametric Statistical Inference". Oxford University Press, 1996. doi:10.1093/oso/9780198523598.001.0001, ISBN 9780198523598.

[74] R. D. Cousins, "Lectures on statistics in theory: prelude to statistics in practice", 2018. arXiv:1807.05996.

[75] T. Junk, "Confidence level computation for combining searches with small statistics", *Nucl. Instrum. Meth. A* **434** (1999) 435, doi:10.1016/S0168-9002(99)00498-2, arXiv:hep-ex/9902006.

[76] A. L. Read, "Presentation of search results: the CL_s technique", *J. Phys. G* **28** (2002) 2693, doi:10.1088/0954-3899/28/10/313.

[77] G. Cowan, K. Cranmer, E. Gross, and O. Vitells, "Asymptotic formulae for likelihood-based tests of new physics", *Eur. Phys. J. C* **71** (2011) 1554, doi:10.1140/epjc/s10052-011-1554-0, arXiv:1007.1727. [Erratum: doi:10.1140/epjc/s10052-013-2501-z].

[78] ATLAS and CMS Collaborations, and LHC Higgs Combination Group, "Procedure for the LHC Higgs boson search combination in Summer 2011", Technical Report CMS-NOTE-2011-005, ATL-PHYS-PUB-2011-11, 2011.

[79] U. Haisch, J. F. Kamenik, A. Malinauskas, and M. Spira, "Collider constraints on light pseudoscalars", *JHEP* **03** (2018) 178, doi:10.1007/JHEP03(2018)178, arXiv:1802.02156.

[80] M. Baumgart and A. Katz, "Implications of a new light scalar near the bottomonium regime", *JHEP* **08** (2012) 133, doi:10.1007/JHEP08(2012)133, arXiv:1204.6032.

A The CMS Collaboration

Yerevan Physics Institute, Yerevan, Armenia
V. Chekhovsky, A. Hayrapetyan, V. Makarenko, A. Tumasyan[1]

Institut für Hochenergiephysik, Vienna, Austria
W. Adam, J.W. Andrejkovic, L. Benato, T. Bergauer, S. Chatterjee, K. Damanakis, M. Dragicevic, P.S. Hussain, M. Jeitler[2], N. Krammer, A. Li, D. Liko, I. Mikulec, J. Schieck[2], R. Schöfbeck[2], D. Schwarz, M. Sonawane, W. Waltenberger, C.-E. Wulz[2]

Universiteit Antwerpen, Antwerpen, Belgium
T. Janssen, H. Kwon, T. Van Laer, P. Van Mechelen

Vrije Universiteit Brussel, Brussel, Belgium
N. Breugelmans, J. D'Hondt, S. Dansana, A. De Moor, M. Delcourt, F. Heyen, Y. Hong, S. Lowette, I. Makarenko, D. Müller, S. Tavernier, M. Tytgat[3], G.P. Van Onsem, S. Van Putte, D. Vannerom

Université Libre de Bruxelles, Bruxelles, Belgium
B. Bilin, B. Clerbaux, A.K. Das, I. De Bruyn, G. De Lentdecker, H. Evard, L. Favart, P. Gianneios, A. Khalilzadeh, F.A. Khan, A. Malara, M.A. Shahzad, L. Thomas, M. Vanden Bemden, C. Vander Velde, P. Vanlaer

Ghent University, Ghent, Belgium
M. De Coen, D. Dobur, G. Gokbulut, J. Knolle, L. Lambrecht, D. Marckx, K. Skovpen, N. Van Den Bossche, J. van der Linden, J. Vandenbroeck, L. Wezenbeek

Université Catholique de Louvain, Louvain-la-Neuve, Belgium
S. Bein, A. Benecke, A. Bethani, G. Bruno, C. Caputo, J. De Favereau De Jeneret, C. Delaere, I.S. Donertas, A. Giammanco, A.O. Guzel, Sa. Jain, V. Lemaitre, J. Lidrych, P. Mastrapasqua, T.T. Tran, S. Turkcapar

Centro Brasileiro de Pesquisas Fisicas, Rio de Janeiro, Brazil
G.A. Alves, E. Coelho, G. Correia Silva, C. Hensel, T. Menezes De Oliveira, C. Mora Herrera[4], P. Rebello Teles, M. Soeiro, E.J. Tonelli Manganote[5], A. Vilela Pereira[4]

Universidade do Estado do Rio de Janeiro, Rio de Janeiro, Brazil
W.L. Aldá Júnior, M. Barroso Ferreira Filho, H. Brandao Malbouisson, W. Carvalho, J. Chinellato[6], E.M. Da Costa, G.G. Da Silveira[7], D. De Jesus Damiao, S. Fonseca De Souza, R. Gomes De Souza, T. Laux Kuhn[7], M. Macedo, J. Martins, K. Mota Amarilo, L. Mundim, H. Nogima, J.P. Pinheiro, A. Santoro, A. Sznajder, M. Thiel

Universidade Estadual Paulista, Universidade Federal do ABC, São Paulo, Brazil
C.A. Bernardes[7], L. Calligaris, T.R. Fernandez Perez Tomei, E.M. Gregores, I. Maietto Silverio, P.G. Mercadante, S.F. Novaes, B. Orzari, Sandra S. Padula, V. Scheurer

Institute for Nuclear Research and Nuclear Energy, Bulgarian Academy of Sciences, Sofia, Bulgaria
A. Aleksandrov, G. Antchev, R. Hadjiiska, P. Iaydjiev, M. Misheva, M. Shopova, G. Sultanov

University of Sofia, Sofia, Bulgaria
A. Dimitrov, L. Litov, B. Pavlov, P. Petkov, A. Petrov, E. Shumka

Instituto De Alta Investigación, Universidad de Tarapacá, Casilla 7 D, Arica, Chile
S. Keshri, D. Laroze, S. Thakur

Beihang University, Beijing, China
T. Cheng, T. Javaid, L. Yuan

Department of Physics, Tsinghua University, Beijing, China
Z. Hu, Z. Liang, J. Liu

Institute of High Energy Physics, Beijing, China
G.M. Chen[8], H.S. Chen[8], M. Chen[8], F. Iemmi, C.H. Jiang, A. Kapoor[9], H. Liao, Z.-A. Liu[10], R. Sharma[11], J.N. Song[10], J. Tao, C. Wang[8], J. Wang, Z. Wang[8], H. Zhang, J. Zhao

State Key Laboratory of Nuclear Physics and Technology, Peking University, Beijing, China
A. Agapitos, Y. Ban, A. Carvalho Antunes De Oliveira, S. Deng, B. Guo, C. Jiang, A. Levin, C. Li, Q. Li, Y. Mao, S. Qian, S.J. Qian, X. Qin, X. Sun, D. Wang, H. Yang, Y. Zhao, C. Zhou

State Key Laboratory of Nuclear Physics and Technology, Institute of Quantum Matter, South China Normal University, Guangzhou, China
S. Yang

Sun Yat-Sen University, Guangzhou, China
Z. You

University of Science and Technology of China, Hefei, China
K. Jaffel, N. Lu

Nanjing Normal University, Nanjing, China
G. Bauer[12], B. Li[13], H. Wang, K. Yi[14], J. Zhang

Institute of Modern Physics and Key Laboratory of Nuclear Physics and Ion-beam Application (MOE) - Fudan University, Shanghai, China
Y. Li

Zhejiang University, Hangzhou, Zhejiang, China
Z. Lin, C. Lu, M. Xiao

Universidad de Los Andes, Bogota, Colombia
C. Avila, D.A. Barbosa Trujillo, A. Cabrera, C. Florez, J. Fraga, J.A. Reyes Vega

Universidad de Antioquia, Medellin, Colombia
J. Jaramillo, C. Rendón, M. Rodriguez, A.A. Ruales Barbosa, J.D. Ruiz Alvarez

University of Split, Faculty of Electrical Engineering, Mechanical Engineering and Naval Architecture, Split, Croatia
D. Giljanovic, N. Godinovic, D. Lelas, A. Sculac

University of Split, Faculty of Science, Split, Croatia
M. Kovac, A. Petkovic, T. Sculac

Institute Rudjer Boskovic, Zagreb, Croatia
P. Bargassa, V. Brigljevic, B.K. Chitroda, D. Ferencek, K. Jakovcic, A. Starodumov[15],

T. Susa

University of Cyprus, Nicosia, Cyprus
A. Attikis, K. Christoforou, A. Hadjiagapiou, C. Leonidou, J. Mousa, C. Nicolaou, L. Paizanos, F. Ptochos, P.A. Razis, H. Rykaczewski, H. Saka, A. Stepennov

Charles University, Prague, Czech Republic
M. Finger, M. Finger Jr., A. Kveton

Escuela Politecnica Nacional, Quito, Ecuador
E. Ayala

Universidad San Francisco de Quito, Quito, Ecuador
E. Carrera Jarrin

Academy of Scientific Research and Technology of the Arab Republic of Egypt, Egyptian Network of High Energy Physics, Cairo, Egypt
B. El-mahdy, S. Khalil[16], E. Salama[17,18]

Center for High Energy Physics (CHEP-FU), Fayoum University, El-Fayoum, Egypt
M. Abdullah Al-Mashad, M.A. Mahmoud

National Institute of Chemical Physics and Biophysics, Tallinn, Estonia
K. Ehataht, M. Kadastik, T. Lange, C. Nielsen, J. Pata, M. Raidal, L. Tani, C. Veelken

Department of Physics, University of Helsinki, Helsinki, Finland
K. Osterberg, M. Voutilainen

Helsinki Institute of Physics, Helsinki, Finland
N. Bin Norjoharuddeen, E. Brücken, F. Garcia, P. Inkaew, K.T.S. Kallonen, T. Lampén, K. Lassila-Perini, S. Lehti, T. Lindén, M. Myllymäki, M.m. Rantanen, J. Tuominiemi

Lappeenranta-Lahti University of Technology, Lappeenranta, Finland
H. Kirschenmann, P. Luukka, H. Petrow

IRFU, CEA, Université Paris-Saclay, Gif-sur-Yvette, France
M. Besancon, F. Couderc, M. Dejardin, D. Denegri, J.L. Faure, F. Ferri, S. Ganjour, P. Gras, G. Hamel de Monchenault, M. Kumar, V. Lohezic, J. Malcles, F. Orlandi, L. Portales, A. Rosowsky, M.Ö. Sahin, A. Savoy-Navarro[19], P. Simkina, M. Titov, M. Tornago

Laboratoire Leprince-Ringuet, CNRS/IN2P3, Ecole Polytechnique, Institut Polytechnique de Paris, Palaiseau, France
F. Beaudette, G. Boldrini, P. Busson, A. Cappati, C. Charlot, M. Chiusi, T.D. Cuisset, F. Damas, O. Davignon, A. De Wit, I.T. Ehle, B.A. Fontana Santos Alves, S. Ghosh, A. Gilbert, R. Granier de Cassagnac, B. Harikrishnan, L. Kalipoliti, G. Liu, M. Manoni, M. Nguyen, S. Obraztsov, C. Ochando, R. Salerno, J.B. Sauvan, Y. Sirois, G. Sokmen, L. Urda Gómez, E. Vernazza, A. Zabi, A. Zghiche

Université de Strasbourg, CNRS, IPHC UMR 7178, Strasbourg, France
J.-L. Agram[20], J. Andrea, D. Bloch, J.-M. Brom, E.C. Chabert, C. Collard, S. Falke, U. Goerlach, R. Haeberle, A.-C. Le Bihan, M. Meena, O. Poncet, G. Saha, M.A. Sessini, P. Van Hove, P. Vaucelle

Centre de Calcul de l'Institut National de Physique Nucleaire et de Physique des Particules, CNRS/IN2P3, Villeurbanne, France
A. Di Florio

Institut de Physique des 2 Infinis de Lyon (IP2I), Villeurbanne, France
D. Amram, S. Beauceron, B. Blancon, G. Boudoul, N. Chanon, D. Contardo, P. Depasse, C. Dozen[21], H. El Mamouni, J. Fay, S. Gascon, M. Gouzevitch, C. Greenberg, G. Grenier, B. Ille, E. Jourd'huy, I.B. Laktineh, M. Lethuillier, L. Mirabito, S. Perries, A. Purohit, M. Vander Donckt, P. Verdier, J. Xiao

Georgian Technical University, Tbilisi, Georgia
G. Adamov, I. Lomidze, Z. Tsamalaidze[15]

RWTH Aachen University, I. Physikalisches Institut, Aachen, Germany
V. Botta, S. Consuegra Rodríguez, L. Feld, K. Klein, M. Lipinski, D. Meuser, A. Pauls, D. Pérez Adán, N. Röwert, M. Teroerde

RWTH Aachen University, III. Physikalisches Institut A, Aachen, Germany
S. Diekmann, A. Dodonova, N. Eich, D. Eliseev, F. Engelke, J. Erdmann, M. Erdmann, B. Fischer, T. Hebbeker, K. Hoepfner, F. Ivone, A. Jung, M.y. Lee, F. Mausolf, M. Merschmeyer, A. Meyer, F. Nowotny, A. Pozdnyakov, Y. Rath, W. Redjeb, F. Rehm, H. Reithler, V. Sarkisovi, A. Schmidt, C. Seth, A. Sharma, J.L. Spah, F. Torres Da Silva De Araujo[22], S. Wiedenbeck, S. Zaleski

RWTH Aachen University, III. Physikalisches Institut B, Aachen, Germany
C. Dziwok, G. Flügge, T. Kress, A. Nowack, O. Pooth, A. Stahl, T. Ziemons, A. Zotz

Deutsches Elektronen-Synchrotron, Hamburg, Germany
H. Aarup Petersen, M. Aldaya Martin, J. Alimena, S. Amoroso, Y. An, J. Bach, S. Baxter, M. Bayatmakou, H. Becerril Gonzalez, O. Behnke, A. Belvedere, F. Blekman[23], K. Borras[24], A. Campbell, A. Cardini, F. Colombina, M. De Silva, G. Eckerlin, D. Eckstein, L.I. Estevez Banos, E. Gallo[23], A. Geiser, V. Guglielmi, M. Guthoff, A. Hinzmann, L. Jeppe, B. Kaech, M. Kasemann, C. Kleinwort, R. Kogler, M. Komm, D. Krücker, W. Lange, D. Leyva Pernia, K. Lipka[25], W. Lohmann[26], F. Lorkowski, R. Mankel, I.-A. Melzer-Pellmann, M. Mendizabal Morentin, A.B. Meyer, G. Milella, K. Moral Figueroa, A. Mussgiller, L.P. Nair, J. Niedziela, A. Nürnberg, J. Park, E. Ranken, A. Raspereza, D. Rastorguev, J. Rübenach, L. Rygaard, M. Scham[27,24], S. Schnake[24], P. Schütze, C. Schwanenberger[23], D. Selivanova, K. Sharko, M. Shchedrolosiev, D. Stafford, F. Vazzoler, A. Ventura Barroso, R. Walsh, D. Wang, Q. Wang, K. Wichmann, L. Wiens[24], C. Wissing, Y. Yang, S. Zakharov, A. Zimermmane Castro Santos

University of Hamburg, Hamburg, Germany
A. Albrecht, S. Albrecht, M. Antonello, S. Bollweg, M. Bonanomi, P. Connor, K. El Morabit, Y. Fischer, E. Garutti, A. Grohsjean, J. Haller, D. Hundhausen, H.R. Jabusch, G. Kasieczka, P. Keicher, R. Klanner, W. Korcari, T. Kramer, C.c. Kuo, V. Kutzner, F. Labe, J. Lange, A. Lobanov, C. Matthies, L. Moureaux, M. Mrowietz, A. Nigamova, Y. Nissan, A. Paasch, K.J. Pena Rodriguez, T. Quadfasel, B. Raciti, M. Rieger, D. Savoiu, J. Schindler, P. Schleper, M. Schröder, J. Schwandt, M. Sommerhalder, H. Stadie, G. Steinbrück, A. Tews, B. Wiederspan, M. Wolf

Karlsruher Institut fuer Technologie, Karlsruhe, Germany
S. Brommer, E. Butz, T. Chwalek, A. Dierlamm, G.G. Dincer, U. Elicabuk, N. Faltermann, M. Giffels, A. Gottmann, F. Hartmann[28], R. Hofsaess, M. Horzela, U. Husemann, J. Kieseler, M. Klute, O. Lavoryk, J.M. Lawhorn, M. Link, A. Lintuluoto, S. Maier, M. Mormile, Th. Müller, M. Neukum, M. Oh, E. Pfeffer, M. Presilla, G. Quast, K. Rabbertz, B. Regnery, R. Schmieder, N. Shadskiy, I. Shvetsov, H.J. Simonis, L. Sowa, L. Stockmeier, K. Tauqeer, M. Toms, B. Topko, N. Trevisani, T. Voigtländer, R.F. Von Cube, J. Von Den Driesch, M. Wassmer, S. Wieland, F. Wittig, R. Wolf, X. Zuo

Institute of Nuclear and Particle Physics (INPP), NCSR Demokritos, Aghia Paraskevi, Greece
G. Anagnostou, G. Daskalakis, A. Kyriakis, A. Papadopoulos[28], A. Stakia

National and Kapodistrian University of Athens, Athens, Greece
G. Melachroinos, Z. Painesis, I. Paraskevas, N. Saoulidou, K. Theofilatos, E. Tziaferi, K. Vellidis, I. Zisopoulos

National Technical University of Athens, Athens, Greece
G. Bakas, T. Chatzistavrou, G. Karapostoli, K. Kousouris, I. Papakrivopoulos, E. Siamarkou, G. Tsipolitis

University of Ioánnina, Ioánnina, Greece
I. Bestintzanos, I. Evangelou, C. Foudas, C. Kamtsikis, P. Katsoulis, P. Kokkas, P.G. Kosmoglou Kioseoglou, N. Manthos, I. Papadopoulos, J. Strologas

HUN-REN Wigner Research Centre for Physics, Budapest, Hungary
C. Hajdu, D. Horvath[29,30], K. Márton, A.J. Rádl[31], F. Sikler, V. Veszpremi

MTA-ELTE Lendület CMS Particle and Nuclear Physics Group, Eötvös Loránd University, Budapest, Hungary
M. Csanád, K. Farkas, A. Fehérkuti[32], M.M.A. Gadallah[33], Á. Kadlecsik, P. Major, G. Pásztor, G.I. Veres

Faculty of Informatics, University of Debrecen, Debrecen, Hungary
B. Ujvari, G. Zilizi

HUN-REN ATOMKI - Institute of Nuclear Research, Debrecen, Hungary
G. Bencze, S. Czellar, J. Molnar, Z. Szillasi

Karoly Robert Campus, MATE Institute of Technology, Gyongyos, Hungary
T. Csorgo[32], F. Nemes[32], T. Novak

Panjab University, Chandigarh, India
S. Bansal, S.B. Beri, V. Bhatnagar, G. Chaudhary, S. Chauhan, N. Dhingra[34], A. Kaur, A. Kaur, H. Kaur, M. Kaur, S. Kumar, T. Sheokand, J.B. Singh, A. Singla

University of Delhi, Delhi, India
A. Bhardwaj, A. Chhetri, B.C. Choudhary, A. Kumar, A. Kumar, M. Naimuddin, K. Ranjan, M.K. Saini, S. Saumya

Indian Institute of Technology Kanpur, Kanpur, India
S. Mukherjee

Saha Institute of Nuclear Physics, HBNI, Kolkata, India

S. Baradia, S. Barman[35], S. Bhattacharya, S. Das Gupta, S. Dutta, S. Dutta, S. Sarkar

Indian Institute of Technology Madras, Madras, India
M.M. Ameen, P.K. Behera, S.C. Behera, S. Chatterjee, G. Dash, P. Jana, P. Kalbhor, S. Kamble, J.R. Komaragiri[36], D. Kumar[36], T. Mishra, B. Parida[37], P.R. Pujahari, N.R. Saha, A.K. Sikdar, R.K. Singh, P. Verma, S. Verma, A. Vijay

Tata Institute of Fundamental Research-A, Mumbai, India
S. Dugad, G.B. Mohanty, M. Shelake, P. Suryadevara

Tata Institute of Fundamental Research-B, Mumbai, India
A. Bala, S. Banerjee, S. Bhowmik[38], R.M. Chatterjee, M. Guchait, Sh. Jain, A. Jaiswal, B.M. Joshi, S. Kumar, G. Majumder, K. Mazumdar, S. Parolia, A. Thachayath

National Institute of Science Education and Research, An OCC of Homi Bhabha National Institute, Bhubaneswar, Odisha, India
S. Bahinipati[39], C. Kar, D. Maity[40], P. Mal, K. Naskar[40], A. Nayak[40], S. Nayak, K. Pal, P. Sadangi, S.K. Swain, S. Varghese[40], D. Vats[40]

Indian Institute of Science Education and Research (IISER), Pune, India
S. Acharya[41], A. Alpana, S. Dube, B. Gomber[41], P. Hazarika, B. Kansal, A. Laha, B. Sahu[41], S. Sharma, K.Y. Vaish

Isfahan University of Technology, Isfahan, Iran
H. Bakhshiansohi[42], A. Jafari[43], M. Zeinali[44]

Institute for Research in Fundamental Sciences (IPM), Tehran, Iran
S. Bashiri, S. Chenarani[45], S.M. Etesami, Y. Hosseini, M. Khakzad, E. Khazaie, M. Mohammadi Najafabadi, S. Tizchang[46]

University College Dublin, Dublin, Ireland
M. Felcini, M. Grunewald

INFN Sezione di Bari[a], Università di Bari[b], Politecnico di Bari[c], Bari, Italy
M. Abbrescia[a,b], A. Colaleo[a,b], D. Creanza[a,c], B. D'Anzi[a,b], N. De Filippis[a,c], M. De Palma[a,b], W. Elmetenawee[a,b,47], N. Ferrara[a,b], L. Fiore[a], G. Iaselli[a,c], L. Longo[a], M. Louka[a,b], G. Maggi[a,c], M. Maggi[a], I. Margjeka[a], V. Mastrapasqua[a,b], S. My[a,b], S. Nuzzo[a,b], A. Pellecchia[a,b], A. Pompili[a,b], G. Pugliese[a,c], R. Radogna[a,b], D. Ramos[a], A. Ranieri[a], L. Silvestris[a], F.M. Simone[a,c], Ü. Sözbilir[a], A. Stamerra[a,b], D. Troiano[a,b], R. Venditti[a,b], P. Verwilligen[a], A. Zaza[a,b]

INFN Sezione di Bologna[a], Università di Bologna[b], Bologna, Italy
G. Abbiendi[a], C. Battilana[a,b], D. Bonacorsi[a,b], P. Capiluppi[a,b], A. Castro[†a,b], F.R. Cavallo[a], M. Cuffiani[a,b], G.M. Dallavalle[a], T. Diotalevi[a,b], F. Fabbri[a], A. Fanfani[a,b], D. Fasanella[a], P. Giacomelli[a], L. Giommi[a,b], C. Grandi[a], L. Guiducci[a,b], S. Lo Meo[a,48], M. Lorusso[a,b], L. Lunerti[a], S. Marcellini[a], G. Masetti[a], F.L. Navarria[a,b], G. Paggi[a,b], A. Perrotta[a], F. Primavera[a,b], A.M. Rossi[a,b], S. Rossi Tisbeni[a,b], T. Rovelli[a,b], G.P. Siroli[a,b]

INFN Sezione di Catania[a], Università di Catania[b], Catania, Italy
S. Costa[a,b,49], A. Di Mattia[a], A. Lapertosa[a], R. Potenza[a,b], A. Tricomi[a,b,49]

INFN Sezione di Firenze[a], Università di Firenze[b], Firenze, Italy

P. Assiouras[a], G. Barbagli[a], G. Bardelli[a,b], M. Bartolini[a,b], B. Camaiani[a,b], A. Cassese[a], R. Ceccarelli[a], V. Ciulli[a,b], C. Civinini[a], R. D'Alessandro[a,b], E. Focardi[a,b], T. Kello[a], G. Latino[a,b], P. Lenzi[a,b], M. Lizzo[a], M. Meschini[a], S. Paoletti[a], A. Papanastassiou[a,b], G. Sguazzoni[a], L. Viliani[a]

INFN Laboratori Nazionali di Frascati, Frascati, Italy
L. Benussi, S. Bianco, S. Meola[50], D. Piccolo

INFN Sezione di Genova[a], Università di Genova[b], Genova, Italy
M. Alves Gallo Pereira[a], F. Ferro[a], E. Robutti[a], S. Tosi[a,b]

INFN Sezione di Milano-Bicocca[a], Università di Milano-Bicocca[b], Milano, Italy
A. Benaglia[a], F. Brivio[a], F. Cetorelli[a,b], F. De Guio[a,b], M.E. Dinardo[a,b], P. Dini[a], S. Gennai[a], R. Gerosa[a,b], A. Ghezzi[a,b], P. Govoni[a,b], L. Guzzi[a], G. Lavizzari[a,b], M.T. Lucchini[a,b], M. Malberti[a], S. Malvezzi[a], A. Massironi[a], D. Menasce[a], L. Moroni[a], M. Paganoni[a,b], S. Palluotto[a,b], D. Pedrini[a], A. Perego[a,b], B.S. Pinolini[a], G. Pizzati[a,b], S. Ragazzi[a,b], T. Tabarelli de Fatis[a,b]

INFN Sezione di Napoli[a], Università di Napoli 'Federico II'[b], Napoli, Italy; Università della Basilicata[c], Potenza, Italy; Scuola Superiore Meridionale (SSM)[d], Napoli, Italy
S. Buontempo[a], A. Cagnotta[a,b], F. Carnevali[a,b], N. Cavallo[a,c], F. Fabozzi[a,c], A.O.M. Iorio[a,b], L. Lista[a,b,51], P. Paolucci[a,28], B. Rossi[a]

INFN Sezione di Padova[a], Università di Padova[b], Padova, Italy; Universita degli Studi di Cagliari[c], Cagliari, Italy
R. Ardino[a], P. Azzi[a], N. Bacchetta[a,52], D. Bisello[a,b], P. Bortignon[a], G. Bortolato[a,b], A.C.M. Bulla[a], R. Carlin[a,b], P. Checchia[a], T. Dorigo[a,53], U. Gasparini[a,b], S. Giorgetti[a], A. Gozzelino[a], M. Gulmini[a,54], E. Lusiani[a], M. Margoni[a,b], M. Migliorini[a,b], J. Pazzini[a,b], P. Ronchese[a,b], R. Rossin[a,b], F. Simonetto[a,b], M. Tosi[a,b], A. Triossi[a,b], S. Ventura[a], M. Zanetti[a,b], P. Zotto[a,b], A. Zucchetta[a,b], G. Zumerle[a,b]

INFN Sezione di Pavia[a], Università di Pavia[b], Pavia, Italy
A. Braghieri[a], S. Calzaferri[a], D. Fiorina[a], P. Montagna[a,b], V. Re[a], C. Riccardi[a,b], P. Salvini[a], I. Vai[a,b], P. Vitulo[a,b]

INFN Sezione di Perugia[a], Università di Perugia[b], Perugia, Italy
S. Ajmal[a,b], M.E. Ascioti[a,b], G.M. Bilei[a], C. Carrivale[a,b], D. Ciangottini[a,b], L. Fanò[a,b], V. Mariani[a,b], M. Menichelli[a], F. Moscatelli[a,55], A. Rossi[a,b], A. Santocchia[a,b], D. Spiga[a], T. Tedeschi[a,b]

INFN Sezione di Pisa[a], Università di Pisa[b], Scuola Normale Superiore di Pisa[c], Pisa, Italy; Università di Siena[d], Siena, Italy
C. Aimè[a], C.A. Alexe[a,c], P. Asenov[a,b], P. Azzurri[a], G. Bagliesi[a], R. Bhattacharya[a], L. Bianchini[a,b], T. Boccali[a], E. Bossini[a], D. Bruschini[a,c], R. Castaldi[a], M.A. Ciocci[a,b], M. Cipriani[a,b], V. D'Amante[a,d], R. Dell'Orso[a], S. Donato[a,b], A. Giassi[a], F. Ligabue[a,c], A.C. Marini[a,b], D. Matos Figueiredo[a], A. Messineo[a,b], S. Mishra[a], V.K. Muraleedharan Nair Bindhu[a,b,40], M. Musich[a,b], S. Nandan[a], F. Palla[a], A. Rizzi[a,b], G. Rolandi[a,c], S. Roy Chowdhury[a], T. Sarkar[a], A. Scribano[a], P. Spagnolo[a], F. Tenchini[a,b], R. Tenchini[a], G. Tonelli[a,b], N. Turini[a,d], F. Vaselli[a,c], A. Venturi[a], P.G. Verdini[a]

INFN Sezione di Roma[a], Sapienza Università di Roma[b], Roma, Italy
P. Barria[a], C. Basile[a,b], F. Cavallari[a], L. Cunqueiro Mendez[a,b], D. Del Re[a,b],

E. Di Marco[a,b], M. Diemoz[a], F. Errico[a,b], R. Gargiulo[a,b], E. Longo[a,b], L. Martikainen[a,b], J. Mijuskovic[a,b], G. Organtini[a,b], F. Pandolfi[a], R. Paramatti[a,b], C. Quaranta[a,b], S. Rahatlou[a,b], C. Rovelli[a], F. Santanastasio[a,b], L. Soffi[a], V. Vladimirov[a,b]

INFN Sezione di Torino[a], Università di Torino[b], Torino, Italy; Università del Piemonte Orientale[c], Novara, Italy
N. Amapane[a,b], R. Arcidiacono[a,c], S. Argiro[a,b], M. Arneodo[a,c], N. Bartosik[a], R. Bellan[a,b], C. Biino[a], C. Borca[a,b], N. Cartiglia[a], M. Costa[a,b], R. Covarelli[a,b], N. Demaria[a], L. Finco[a], M. Grippo[a,b], B. Kiani[a,b], F. Legger[a], F. Luongo[a,b], C. Mariotti[a], L. Markovic[a,b], S. Maselli[a], A. Mecca[a,b], L. Menzio[a,b], P. Meridiani[a], E. Migliore[a,b], M. Monteno[a], R. Mulargia[a], M.M. Obertino[a,b], G. Ortona[a], L. Pacher[a,b], N. Pastrone[a], M. Pelliccioni[a], M. Ruspa[a,c], F. Siviero[a,b], V. Sola[a,b], A. Solano[a,b], A. Staiano[a], C. Tarricone[a,b], D. Trocino[a], G. Umoret[a,b], R. White[a,b]

INFN Sezione di Trieste[a], Università di Trieste[b], Trieste, Italy
J. Babbar[a,b], S. Belforte[a], V. Candelise[a,b], M. Casarsa[a], F. Cossutti[a], K. De Leo[a], G. Della Ricca[a,b]

Kyungpook National University, Daegu, Korea
S. Dogra, J. Hong, J. Kim, D. Lee, H. Lee, S.W. Lee, C.S. Moon, Y.D. Oh, M.S. Ryu, S. Sekmen, B. Tae, Y.C. Yang

Department of Mathematics and Physics - GWNU, Gangneung, Korea
M.S. Kim

Chonnam National University, Institute for Universe and Elementary Particles, Kwangju, Korea
G. Bak, P. Gwak, H. Kim, D.H. Moon

Hanyang University, Seoul, Korea
E. Asilar, J. Choi[56], D. Kim, T.J. Kim, J.A. Merlin, Y. Ryou

Korea University, Seoul, Korea
S. Choi, S. Han, B. Hong, K. Lee, K.S. Lee, S. Lee, J. Yoo

Kyung Hee University, Department of Physics, Seoul, Korea
J. Goh, S. Yang

Sejong University, Seoul, Korea
Y. Kang, H. S. Kim, Y. Kim, S. Lee

Seoul National University, Seoul, Korea
J. Almond, J.H. Bhyun, J. Choi, J. Choi, W. Jun, J. Kim, Y.W. Kim, S. Ko, H. Lee, J. Lee, J. Lee, B.H. Oh, S.B. Oh, H. Seo, U.K. Yang, I. Yoon

University of Seoul, Seoul, Korea
W. Jang, D.Y. Kang, S. Kim, B. Ko, J.S.H. Lee, Y. Lee, I.C. Park, Y. Roh, I.J. Watson

Yonsei University, Department of Physics, Seoul, Korea
S. Ha, K. Hwang, B. Kim, K. Lee, H.D. Yoo

Sungkyunkwan University, Suwon, Korea
M. Choi, M.R. Kim, H. Lee, Y. Lee, I. Yu

College of Engineering and Technology, American University of the Middle East (AUM),

Dasman, Kuwait
T. Beyrouthy, Y. Gharbia

Kuwait University - College of Science - Department of Physics, Safat, Kuwait
F. Alazemi

Riga Technical University, Riga, Latvia
K. Dreimanis, A. Gaile, C. Munoz Diaz, D. Osite, G. Pikurs, A. Potrebko, M. Seidel, D. Sidiropoulos Kontos

University of Latvia (LU), Riga, Latvia
N.R. Strautnieks

Vilnius University, Vilnius, Lithuania
M. Ambrozas, A. Juodagalvis, A. Rinkevicius, G. Tamulaitis

National Centre for Particle Physics, Universiti Malaya, Kuala Lumpur, Malaysia
I. Yusuff[57], Z. Zolkapli

Universidad de Sonora (UNISON), Hermosillo, Mexico
J.F. Benitez, A. Castaneda Hernandez, H.A. Encinas Acosta, L.G. Gallegos Maríñez, M. León Coello, J.A. Murillo Quijada, A. Sehrawat, L. Valencia Palomo

Centro de Investigacion y de Estudios Avanzados del IPN, Mexico City, Mexico
G. Ayala, H. Castilla-Valdez, H. Crotte Ledesma, E. De La Cruz-Burelo, I. Heredia-De La Cruz[58], R. Lopez-Fernandez, J. Mejia Guisao, A. Sánchez Hernández

Universidad Iberoamericana, Mexico City, Mexico
C. Oropeza Barrera, D.L. Ramirez Guadarrama, M. Ramírez García

Benemerita Universidad Autonoma de Puebla, Puebla, Mexico
I. Bautista, F.E. Neri Huerta, I. Pedraza, H.A. Salazar Ibarguen, C. Uribe Estrada

University of Montenegro, Podgorica, Montenegro
I. Bubanja, N. Raicevic

University of Canterbury, Christchurch, New Zealand
P.H. Butler

National Centre for Physics, Quaid-I-Azam University, Islamabad, Pakistan
A. Ahmad, M.I. Asghar, A. Awais, M.I.M. Awan, H.R. Hoorani, W.A. Khan

AGH University of Krakow, Krakow, Poland
V. Avati, A. Bellora, L. Forthomme, L. Grzanka, M. Malawski, K. Piotrzkowski

National Centre for Nuclear Research, Swierk, Poland
H. Bialkowska, M. Bluj, M. Górski, M. Kazana, M. Szleper, P. Zalewski

Institute of Experimental Physics, Faculty of Physics, University of Warsaw, Warsaw, Poland
K. Bunkowski, K. Doroba, A. Kalinowski, M. Konecki, J. Krolikowski, A. Muhammad

Warsaw University of Technology, Warsaw, Poland
P. Fokow, K. Pozniak, W. Zabolotny

Laboratório de Instrumentação e Física Experimental de Partículas, Lisboa, Portugal
M. Araujo, D. Bastos, C. Beirão Da Cruz E Silva, A. Boletti, M. Bozzo, T. Camporesi, G. Da Molin, P. Faccioli, M. Gallinaro, J. Hollar, N. Leonardo,

G.B. Marozzo, A. Petrilli, M. Pisano, J. Seixas, J. Varela, J.W. Wulff

Faculty of Physics, University of Belgrade, Belgrade, Serbia
P. Adzic, P. Milenovic

VINCA Institute of Nuclear Sciences, University of Belgrade, Belgrade, Serbia
D. Devetak, M. Dordevic, J. Milosevic, L. Nadderd, V. Rekovic, M. Stojanovic

Centro de Investigaciones Energéticas Medioambientales y Tecnológicas (CIEMAT), Madrid, Spain
J. Alcaraz Maestre, Cristina F. Bedoya, J.A. Brochero Cifuentes, Oliver M. Carretero, M. Cepeda, M. Cerrada, N. Colino, B. De La Cruz, A. Delgado Peris, A. Escalante Del Valle, D. Fernández Del Val, J.P. Fernández Ramos, J. Flix, M.C. Fouz, O. Gonzalez Lopez, S. Goy Lopez, J.M. Hernandez, M.I. Josa, J. Llorente Merino, C. Martin Perez, E. Martin Viscasillas, D. Moran, C. M. Morcillo Perez, Á. Navarro Tobar, C. Perez Dengra, A. Pérez-Calero Yzquierdo, J. Puerta Pelayo, I. Redondo, J. Sastre, J. Vazquez Escobar

Universidad Autónoma de Madrid, Madrid, Spain
J.F. de Trocóniz

Universidad de Oviedo, Instituto Universitario de Ciencias y Tecnologías Espaciales de Asturias (ICTEA), Oviedo, Spain
B. Alvarez Gonzalez, J. Cuevas, J. Fernandez Menendez, S. Folgueras, I. Gonzalez Caballero, P. Leguina, E. Palencia Cortezon, J. Prado Pico, V. Rodríguez Bouza, A. Soto Rodríguez, A. Trapote, C. Vico Villalba, P. Vischia

Instituto de Física de Cantabria (IFCA), CSIC-Universidad de Cantabria, Santander, Spain
S. Blanco Fernández, I.J. Cabrillo, A. Calderon, J. Duarte Campderros, M. Fernandez, G. Gomez, C. Lasaosa García, R. Lopez Ruiz, C. Martinez Rivero, P. Martinez Ruiz del Arbol, F. Matorras, P. Matorras Cuevas, E. Navarrete Ramos, J. Piedra Gomez, L. Scodellaro, I. Vila, J.M. Vizan Garcia

University of Colombo, Colombo, Sri Lanka
B. Kailasapathy[59], D.D.C. Wickramarathna

University of Ruhuna, Department of Physics, Matara, Sri Lanka
W.G.D. Dharmaratna[60], K. Liyanage, N. Perera

CERN, European Organization for Nuclear Research, Geneva, Switzerland
D. Abbaneo, C. Amendola, E. Auffray, J. Baechler, D. Barney, A. Bermúdez Martínez, M. Bianco, A.A. Bin Anuar, A. Bocci, L. Borgonovi, C. Botta, A. Bragagnolo, E. Brondolin, C.E. Brown, C. Caillol, G. Cerminara, N. Chernyavskaya, D. d'Enterria, A. Dabrowski, A. David, A. De Roeck, M.M. Defranchis, M. Deile, M. Dobson, G. Franzoni, W. Funk, S. Giani, D. Gigi, K. Gill, F. Glege, M. Glowacki, J. Hegeman, J.K. Heikkilä, B. Huber, V. Innocente, T. James, P. Janot, O. Kaluzinska, O. Karacheban[26], G. Karathanasis, S. Laurila, P. Lecoq, E. Leutgeb, C. Lourenço, M. Magherini, L. Malgeri, M. Mannelli, M. Matthewman, A. Mehta, F. Meijers, S. Mersi, E. Meschi, V. Milosevic, F. Monti, F. Moortgat, M. Mulders, I. Neutelings, S. Orfanelli, F. Pantaleo, G. Petrucciani, A. Pfeiffer, M. Pierini, M. Pitt, H. Qu, D. Rabady, B. Ribeiro Lopes, F. Riti, M. Rovere, H. Sakulin, R. Salvatico, S. Sanchez Cruz, S. Scarfi, M. Selvaggi, A. Sharma, K. Shchelina, P. Silva, P. Sphicas[61], A.G. Stahl Leiton, A. Steen, S. Summers, D. Treille, P. Tropea, D. Walter,

J. Wanczyk[62], J. Wang, S. Wuchterl, P. Zehetner, P. Zejdl, W.D. Zeuner

PSI Center for Neutron and Muon Sciences, Villigen, Switzerland
T. Bevilacqua[63], L. Caminada[63], A. Ebrahimi, W. Erdmann, R. Horisberger, Q. Ingram, H.C. Kaestli, D. Kotlinski, C. Lange, M. Missiroli[63], L. Noehte[63], T. Rohe, A. Samalan

ETH Zurich - Institute for Particle Physics and Astrophysics (IPA), Zurich, Switzerland
T.K. Aarrestad, M. Backhaus, G. Bonomelli, A. Calandri, C. Cazzaniga, K. Datta, P. De Bryas Dexmiers D'archiac[62], A. De Cosa, G. Dissertori, M. Dittmar, M. Donegà, F. Eble, M. Galli, K. Gedia, F. Glessgen, C. Grab, N. Härringer, T.G. Harte, D. Hits, W. Lustermann, A.-M. Lyon, R.A. Manzoni, M. Marchegiani, L. Marchese, A. Mascellani[62], F. Nessi-Tedaldi, F. Pauss, V. Perovic, S. Pigazzini, B. Ristic, R. Seidita, J. Steggemann[62], A. Tarabini, D. Valsecchi, R. Wallny

Universität Zürich, Zurich, Switzerland
C. Amsler[64], P. Bärtschi, M.F. Canelli, K. Cormier, M. Huwiler, W. Jin, A. Jofrehei, B. Kilminster, S. Leontsinis, S.P. Liechti, A. Macchiolo, P. Meiring, F. Meng, J. Motta, A. Reimers, P. Robmann, M. Senger, E. Shokr, F. Stäger, R. Tramontano

National Central University, Chung-Li, Taiwan
C. Adloff[65], D. Bhowmik, C.M. Kuo, W. Lin, P.K. Rout, P.C. Tiwari[36]

National Taiwan University (NTU), Taipei, Taiwan
L. Ceard, K.F. Chen, Z.g. Chen, A. De Iorio, W.-S. Hou, T.h. Hsu, Y.w. Kao, S. Karmakar, G. Kole, Y.y. Li, R.-S. Lu, E. Paganis, X.f. Su, J. Thomas-Wilsker, L.s. Tsai, D. Tsionou, H.y. Wu, E. Yazgan

High Energy Physics Research Unit, Department of Physics, Faculty of Science, Chulalongkorn University, Bangkok, Thailand
C. Asawatangtrakuldee, N. Srimanobhas, V. Wachirapusitanand

Tunis El Manar University, Tunis, Tunisia
Y. Maghrbi

Çukurova University, Physics Department, Science and Art Faculty, Adana, Turkey
D. Agyel, F. Boran, F. Dolek, I. Dumanoglu[66], E. Eskut, Y. Guler[67], E. Gurpinar Guler[67], C. Isik, O. Kara, A. Kayis Topaksu, Y. Komurcu, G. Onengut, K. Ozdemir[68], A. Polatoz, B. Tali[69], U.G. Tok, E. Uslan, I.S. Zorbakir

Middle East Technical University, Physics Department, Ankara, Turkey
M. Yalvac[70]

Bogazici University, Istanbul, Turkey
B. Akgun, I.O. Atakisi, E. Gülmez, M. Kaya[71], O. Kaya[72], S. Tekten[73]

Istanbul Technical University, Istanbul, Turkey
A. Cakir, K. Cankocak[66,74], S. Sen[75]

Istanbul University, Istanbul, Turkey
O. Aydilek[76], B. Hacisahinoglu, I. Hos[77], B. Kaynak, S. Ozkorucuklu, O. Potok, H. Sert, C. Simsek, C. Zorbilmez

Yildiz Technical University, Istanbul, Turkey

S. Cerci, B. Isildak[78], D. Sunar Cerci, T. Yetkin

Institute for Scintillation Materials of National Academy of Science of Ukraine, Kharkiv, Ukraine
A. Boyaryntsev, B. Grynyov

National Science Centre, Kharkiv Institute of Physics and Technology, Kharkiv, Ukraine
L. Levchuk

University of Bristol, Bristol, United Kingdom
D. Anthony, J.J. Brooke, A. Bundock, F. Bury, E. Clement, D. Cussans, H. Flacher, J. Goldstein, H.F. Heath, M.-L. Holmberg, L. Kreczko, S. Paramesvaran, L. Robertshaw, V.J. Smith, K. Walkingshaw Pass

Rutherford Appleton Laboratory, Didcot, United Kingdom
A.H. Ball, K.W. Bell, A. Belyaev[79], C. Brew, R.M. Brown, D.J.A. Cockerill, C. Cooke, A. Elliot, K.V. Ellis, K. Harder, S. Harper, J. Linacre, K. Manolopoulos, D.M. Newbold, E. Olaiya, D. Petyt, T. Reis, A.R. Sahasransu, G. Salvi, T. Schuh, C.H. Shepherd-Themistocleous, I.R. Tomalin, K.C. Whalen, T. Williams

Imperial College, London, United Kingdom
I. Andreou, R. Bainbridge, P. Bloch, O. Buchmuller, C.A. Carrillo Montoya, G.S. Chahal[80], D. Colling, J.S. Dancu, I. Das, P. Dauncey, G. Davies, M. Della Negra, S. Fayer, G. Fedi, G. Hall, A. Howard, G. Iles, C.R. Knight, P. Krueper, J. Langford, K.H. Law, J. León Holgado, L. Lyons, A.-M. Magnan, B. Maier, S. Mallios, M. Mieskolainen, J. Nash[81], M. Pesaresi, P.B. Pradeep, B.C. Radburn-Smith, A. Richards, A. Rose, K. Savva, C. Seez, R. Shukla, A. Tapper, K. Uchida, G.P. Uttley, T. Virdee[28], M. Vojinovic, N. Wardle, D. Winterbottom

Brunel University, Uxbridge, United Kingdom
J.E. Cole, A. Khan, P. Kyberd, I.D. Reid

Baylor University, Waco, Texas, USA
S. Abdullin, A. Brinkerhoff, E. Collins, M.R. Darwish, J. Dittmann, K. Hatakeyama, V. Hegde, J. Hiltbrand, B. McMaster, J. Samudio, S. Sawant, C. Sutantawibul, J. Wilson

Catholic University of America, Washington, DC, USA
R. Bartek, A. Dominguez, A.E. Simsek, S.S. Yu

The University of Alabama, Tuscaloosa, Alabama, USA
B. Bam, A. Buchot Perraguin, R. Chudasama, S.I. Cooper, C. Crovella, S.V. Gleyzer, E. Pearson, C.U. Perez, P. Rumerio[82], E. Usai, R. Yi

Boston University, Boston, Massachusetts, USA
A. Akpinar, C. Cosby, G. De Castro, Z. Demiragli, C. Erice, C. Fangmeier, C. Fernandez Madrazo, E. Fontanesi, D. Gastler, F. Golf, S. Jeon, J. O'cain, I. Reed, J. Rohlf, K. Salyer, D. Sperka, D. Spitzbart, I. Suarez, A. Tsatsos, A.G. Zecchinelli

Brown University, Providence, Rhode Island, USA
G. Barone, G. Benelli, D. Cutts, S. Ellis, L. Gouskos, M. Hadley, U. Heintz, K.W. Ho, J.M. Hogan[83], T. Kwon, G. Landsberg, K.T. Lau, J. Luo, S. Mondal, T. Russell, S. Sagir[84], X. Shen, M. Stamenkovic, N. Venkatasubramanian

University of California, Davis, Davis, California, USA
S. Abbott, B. Barton, C. Brainerd, R. Breedon, H. Cai, M. Calderon De La Barca Sanchez, M. Chertok, M. Citron, J. Conway, P.T. Cox, R. Erbacher, F. Jensen, O. Kukral, G. Mocellin, M. Mulhearn, S. Ostrom, W. Wei, S. Yoo, F. Zhang

University of California, Los Angeles, California, USA
K. Adamidis, M. Bachtis, D. Campos, R. Cousins, A. Datta, G. Flores Avila, J. Hauser, M. Ignatenko, M.A. Iqbal, T. Lam, Y.f. Lo, E. Manca, A. Nunez Del Prado, D. Saltzberg, V. Valuev

University of California, Riverside, Riverside, California, USA
R. Clare, J.W. Gary, G. Hanson

University of California, San Diego, La Jolla, California, USA
A. Aportela, A. Arora, J.G. Branson, S. Cittolin, S. Cooperstein, D. Diaz, J. Duarte, L. Giannini, Y. Gu, J. Guiang, R. Kansal, V. Krutelyov, R. Lee, J. Letts, M. Masciovecchio, F. Mokhtar, S. Mukherjee, M. Pieri, D. Primosch, M. Quinnan, V. Sharma, M. Tadel, E. Vourliotis, F. Würthwein, Y. Xiang, A. Yagil

University of California, Santa Barbara - Department of Physics, Santa Barbara, California, USA
A. Barzdukas, L. Brennan, C. Campagnari, K. Downham, C. Grieco, M.M. Hussain, J. Incandela, J. Kim, A.J. Li, P. Masterson, H. Mei, J. Richman, S.N. Santpur, U. Sarica, R. Schmitz, F. Setti, J. Sheplock, D. Stuart, T.Á. Vámi, X. Yan, D. Zhang

California Institute of Technology, Pasadena, California, USA
S. Bhattacharya, A. Bornheim, O. Cerri, J. Mao, H.B. Newman, G. Reales Gutiérrez, M. Spiropulu, J.R. Vlimant, C. Wang, S. Xie, R.Y. Zhu

Carnegie Mellon University, Pittsburgh, Pennsylvania, USA
J. Alison, S. An, P. Bryant, M. Cremonesi, V. Dutta, T. Ferguson, T.A. Gómez Espinosa, A. Harilal, A. Kallil Tharayil, M. Kanemura, C. Liu, T. Mudholkar, S. Murthy, P. Palit, K. Park, M. Paulini, A. Roberts, A. Sanchez, W. Terrill

University of Colorado Boulder, Boulder, Colorado, USA
J.P. Cumalat, W.T. Ford, A. Hart, A. Hassani, N. Manganelli, J. Pearkes, C. Savard, N. Schonbeck, K. Stenson, K.A. Ulmer, S.R. Wagner, N. Zipper, D. Zuolo

Cornell University, Ithaca, New York, USA
J. Alexander, X. Chen, D.J. Cranshaw, J. Dickinson, J. Fan, X. Fan, S. Hogan, P. Kotamnives, J. Monroy, M. Oshiro, J.R. Patterson, M. Reid, A. Ryd, J. Thom, P. Wittich, R. Zou

Fermi National Accelerator Laboratory, Batavia, Illinois, USA
M. Albrow, M. Alyari, O. Amram, G. Apollinari, A. Apresyan, L.A.T. Bauerdick, D. Berry, J. Berryhill, P.C. Bhat, K. Burkett, J.N. Butler, A. Canepa, G.B. Cerati, H.W.K. Cheung, F. Chlebana, G. Cummings, I. Dutta, V.D. Elvira, J. Freeman, A. Gandrakota, Z. Gecse, L. Gray, D. Green, A. Grummer, S. Grünendahl, D. Guerrero, O. Gutsche, R.M. Harris, T.C. Herwig, J. Hirschauer, B. Jayatilaka, S. Jindariani, M. Johnson, U. Joshi, T. Klijnsma, B. Klima, K.H.M. Kwok,

S. Lammel, C. Lee, D. Lincoln, R. Lipton, T. Liu, K. Maeshima, D. Mason, P. McBride, P. Merkel, S. Mrenna, S. Nahn, J. Ngadiuba, D. Noonan, S. Norberg, V. Papadimitriou, N. Pastika, K. Pedro, C. Pena[85], F. Ravera, A. Reinsvold Hall[86], L. Ristori, M. Safdari, E. Sexton-Kennedy, N. Smith, A. Soha, L. Spiegel, S. Stoynev, J. Strait, L. Taylor, S. Tkaczyk, N.V. Tran, L. Uplegger, E.W. Vaandering, I. Zoi

University of Florida, Gainesville, Florida, USA
C. Aruta, P. Avery, D. Bourilkov, P. Chang, V. Cherepanov, R.D. Field, C. Huh, E. Koenig, M. Kolosova, J. Konigsberg, A. Korytov, K. Matchev, N. Menendez, G. Mitselmakher, K. Mohrman, A. Muthirakalayil Madhu, N. Rawal, S. Rosenzweig, Y. Takahashi, J. Wang

Florida State University, Tallahassee, Florida, USA
T. Adams, A. Al Kadhim, A. Askew, S. Bower, R. Hashmi, R.S. Kim, S. Kim, T. Kolberg, G. Martinez, H. Prosper, P.R. Prova, M. Wulansatiti, R. Yohay, J. Zhang

Florida Institute of Technology, Melbourne, Florida, USA
B. Alsufyani, S. Butalla, S. Das, T. Elkafrawy[18], M. Hohlmann, E. Yanes

University of Illinois Chicago, Chicago, Illinois, USA
M.R. Adams, A. Baty, C. Bennett, R. Cavanaugh, R. Escobar Franco, O. Evdokimov, C.E. Gerber, H. Gupta, M. Hawksworth, A. Hingrajiya, D.J. Hofman, J.h. Lee, D. S. Lemos, C. Mills, S. Nanda, G. Oh, B. Ozek, D. Pilipovic, R. Pradhan, E. Prifti, P. Roy, T. Roy, S. Rudrabhatla, N. Singh, M.B. Tonjes, N. Varelas, M.A. Wadud, Z. Ye, J. Yoo

The University of Iowa, Iowa City, Iowa, USA
M. Alhusseini, D. Blend, K. Dilsiz[87], L. Emediato, G. Karaman, O.K. Köseyan, J.-P. Merlo, A. Mestvirishvili[88], O. Neogi, H. Ogul[89], Y. Onel, A. Penzo, C. Snyder, E. Tiras[90]

Johns Hopkins University, Baltimore, Maryland, USA
B. Blumenfeld, L. Corcodilos, J. Davis, A.V. Gritsan, L. Kang, S. Kyriacou, P. Maksimovic, M. Roguljic, J. Roskes, S. Sekhar, M. Swartz

The University of Kansas, Lawrence, Kansas, USA
A. Abreu, L.F. Alcerro Alcerro, J. Anguiano, S. Arteaga Escatel, P. Baringer, A. Bean, Z. Flowers, D. Grove, J. King, G. Krintiras, M. Lazarovits, C. Le Mahieu, J. Marquez, M. Murray, M. Nickel, S. Popescu[91], C. Rogan, C. Royon, S. Sanders, C. Smith, G. Wilson

Kansas State University, Manhattan, Kansas, USA
B. Allmond, R. Gujju Gurunadha, A. Ivanov, K. Kaadze, Y. Maravin, J. Natoli, D. Roy, G. Sorrentino

University of Maryland, College Park, Maryland, USA
A. Baden, A. Belloni, J. Bistany-riebman, Y.M. Chen, S.C. Eno, N.J. Hadley, S. Jabeen, R.G. Kellogg, T. Koeth, B. Kronheim, S. Lascio, A.C. Mignerey, S. Nabili, C. Palmer, C. Papageorgakis, M.M. Paranjpe, E. Popova[92], A. Shevelev, L. Wang, L. Zhang

Massachusetts Institute of Technology, Cambridge, Massachusetts, USA
C. Baldenegro Barrera, J. Bendavid, S. Bright-Thonney, I.A. Cali, P.c. Chou,

M. D'Alfonso, J. Eysermans, C. Freer, G. Gomez-Ceballos, M. Goncharov, G. Grosso, P. Harris, D. Hoang, D. Kovalskyi, J. Krupa, L. Lavezzo, Y.-J. Lee, K. Long, C. Mcginn, A. Novak, M.I. Park, C. Paus, C. Reissel, C. Roland, G. Roland, S. Rothman, G.S.F. Stephans, Z. Wang, B. Wyslouch, T. J. Yang

University of Minnesota, Minneapolis, Minnesota, USA
B. Crossman, C. Kapsiak, M. Krohn, D. Mahon, J. Mans, B. Marzocchi, M. Revering, R. Rusack, R. Saradhy, N. Strobbe

University of Nebraska-Lincoln, Lincoln, Nebraska, USA
K. Bloom, D.R. Claes, G. Haza, J. Hossain, C. Joo, I. Kravchenko, A. Rohilla, J.E. Siado, W. Tabb, A. Vagnerini, A. Wightman, F. Yan, D. Yu

State University of New York at Buffalo, Buffalo, New York, USA
H. Bandyopadhyay, L. Hay, H.w. Hsia, I. Iashvili, A. Kalogeropoulos, A. Kharchilava, M. Morris, D. Nguyen, S. Rappoccio, H. Rejeb Sfar, A. Williams, P. Young

Northeastern University, Boston, Massachusetts, USA
G. Alverson, E. Barberis, J. Bonilla, B. Bylsma, M. Campana, J. Dervan, Y. Haddad, Y. Han, I. Israr, A. Krishna, P. Levchenko, J. Li, M. Lu, R. Mccarthy, D.M. Morse, T. Orimoto, A. Parker, L. Skinnari, E. Tsai, D. Wood

Northwestern University, Evanston, Illinois, USA
S. Dittmer, K.A. Hahn, D. Li, Y. Liu, M. Mcginnis, Y. Miao, D.G. Monk, M.H. Schmitt, A. Taliercio, M. Velasco

University of Notre Dame, Notre Dame, Indiana, USA
G. Agarwal, R. Band, R. Bucci, S. Castells, A. Das, R. Goldouzian, M. Hildreth, K. Hurtado Anampa, T. Ivanov, C. Jessop, K. Lannon, J. Lawrence, N. Loukas, L. Lutton, J. Mariano, N. Marinelli, I. Mcalister, T. McCauley, C. Mcgrady, C. Moore, Y. Musienko[15], H. Nelson, M. Osherson, A. Piccinelli, R. Ruchti, A. Townsend, Y. Wan, M. Wayne, H. Yockey, M. Zarucki, L. Zygala

The Ohio State University, Columbus, Ohio, USA
A. Basnet, M. Carrigan, L.S. Durkin, C. Hill, M. Joyce, M. Nunez Ornelas, K. Wei, D.A. Wenzl, B.L. Winer, B. R. Yates

Princeton University, Princeton, New Jersey, USA
H. Bouchamaoui, K. Coldham, P. Das, G. Dezoort, P. Elmer, P. Fackeldey, A. Frankenthal, B. Greenberg, N. Haubrich, K. Kennedy, G. Kopp, S. Kwan, Y. Lai, D. Lange, A. Loeliger, D. Marlow, I. Ojalvo, J. Olsen, F. Simpson, D. Stickland, C. Tully, L.H. Vage

University of Puerto Rico, Mayaguez, Puerto Rico, USA
S. Malik, R. Sharma

Purdue University, West Lafayette, Indiana, USA
A.S. Bakshi, S. Chandra, R. Chawla, A. Gu, L. Gutay, M. Jones, A.W. Jung, A.M. Koshy, M. Liu, G. Negro, N. Neumeister, G. Paspalaki, S. Piperov, J.F. Schulte, A. K. Virdi, F. Wang, A. Wildridge, W. Xie, Y. Yao

Purdue University Northwest, Hammond, Indiana, USA
J. Dolen, N. Parashar, A. Pathak

Rice University, Houston, Texas, USA
D. Acosta, A. Agrawal, T. Carnahan, K.M. Ecklund, P.J. Fernández Manteca, S. Freed, P. Gardner, F.J.M. Geurts, I. Krommydas, W. Li, J. Lin, O. Miguel Colin, B.P. Padley, R. Redjimi, J. Rotter, E. Yigitbasi, Y. Zhang

University of Rochester, Rochester, New York, USA
A. Bodek, P. de Barbaro, R. Demina, J.L. Dulemba, A. Garcia-Bellido, O. Hindrichs, A. Khukhunaishvili, N. Parmar, P. Parygin[92], R. Taus

Rutgers, The State University of New Jersey, Piscataway, New Jersey, USA
B. Chiarito, J.P. Chou, S.V. Clark, D. Gadkari, Y. Gershtein, E. Halkiadakis, M. Heindl, C. Houghton, D. Jaroslawski, S. Konstantinou, I. Laflotte, A. Lath, R. Montalvo, K. Nash, J. Reichert, P. Saha, S. Salur, S. Schnetzer, S. Somalwar, R. Stone, S.A. Thayil, S. Thomas, J. Vora

University of Tennessee, Knoxville, Tennessee, USA
D. Ally, A.G. Delannoy, S. Fiorendi, S. Higginbotham, T. Holmes, A.R. Kanuganti, N. Karunarathna, L. Lee, E. Nibigira, S. Spanier

Texas A&M University, College Station, Texas, USA
D. Aebi, M. Ahmad, T. Akhter, K. Androsov[62], O. Bouhali[93], R. Eusebi, J. Gilmore, T. Huang, T. Kamon[94], H. Kim, S. Luo, R. Mueller, D. Overton, A. Safonov

Texas Tech University, Lubbock, Texas, USA
N. Akchurin, J. Damgov, Y. Feng, N. Gogate, Y. Kazhykarim, K. Lamichhane, S.W. Lee, C. Madrid, A. Mankel, T. Peltola, I. Volobouev

Vanderbilt University, Nashville, Tennessee, USA
E. Appelt, Y. Chen, S. Greene, A. Gurrola, W. Johns, R. Kunnawalkam Elayavalli, A. Melo, D. Rathjens, F. Romeo, P. Sheldon, S. Tuo, J. Velkovska, J. Viinikainen

University of Virginia, Charlottesville, Virginia, USA
B. Cardwell, H. Chung, B. Cox, J. Hakala, R. Hirosky, A. Ledovskoy, C. Mantilla, C. Neu, C. Ramón Álvarez

Wayne State University, Detroit, Michigan, USA
S. Bhattacharya, P.E. Karchin

University of Wisconsin - Madison, Madison, Wisconsin, USA
A. Aravind, S. Banerjee, K. Black, T. Bose, E. Chavez, S. Dasu, P. Everaerts, C. Galloni, H. He, M. Herndon, A. Herve, C.K. Koraka, A. Lanaro, R. Loveless, J. Madhusudanan Sreekala, A. Mallampalli, A. Mohammadi, S. Mondal, G. Parida, L. Pétré, D. Pinna, A. Savin, V. Shang, V. Sharma, W.H. Smith, D. Teague, H.F. Tsoi, W. Vetens, A. Warden

Authors affiliated with an international laboratory covered by a cooperation agreement with CERN
S. Afanasiev, V. Alexakhin, D. Budkouski, I. Golutvin†, I. Gorbunov, V. Karjavine, O. Kodolova[95,92], V. Korenkov, A. Lanev, A. Malakhov, V. Matveev[96], A. Nikitenko[97,95], V. Palichik, V. Perelygin, M. Savina, V. Shalaev, S. Shmatov, S. Shulha, V. Smirnov, O. Teryaev, N. Voytishin, B.S. Yuldashev†[98], A. Zarubin, I. Zhizhin

Authors affiliated with an institute formerly covered by a cooperation agreement with CERN

G. Gavrilov, V. Golovtcov, Y. Ivanov, V. Kim[96], V. Murzin, V. Oreshkin, D. Sosnov, V. Sulimov, L. Uvarov, A. Vorobyev†, Yu. Andreev, A. Dermenev, S. Gninenko, N. Golubev, A. Karneyeu, D. Kirpichnikov, M. Kirsanov, N. Krasnikov, I. Tlisova, A. Toropin, T. Aushev, K. Ivanov, V. Gavrilov, N. Lychkovskaya, V. Popov, A. Zhokin, M. Chadeeva[96], R. Chistov[96], S. Polikarpov[96], V. Andreev, M. Azarkin, M. Kirakosyan, A. Terkulov, E. Boos, V. Bunichev, M. Dubinin[85], L. Dudko, A. Gribushin, V. Klyukhin, M. Perfilov, V. Savrin, P. Volkov, G. Vorotnikov, V. Blinov[96], T. Dimova[96], A. Kozyrev[96], O. Radchenko[96], Y. Skovpen[96], V. Kachanov, S. Slabospitskii, A. Uzunian, A. Babaev, V. Borshch, D. Druzhkin

†: Deceased
[1]Also at Yerevan State University, Yerevan, Armenia
[2]Also at TU Wien, Vienna, Austria
[3]Also at Ghent University, Ghent, Belgium
[4]Also at Universidade do Estado do Rio de Janeiro, Rio de Janeiro, Brazil
[5]Also at FACAMP - Faculdades de Campinas, Sao Paulo, Brazil
[6]Also at Universidade Estadual de Campinas, Campinas, Brazil
[7]Also at Federal University of Rio Grande do Sul, Porto Alegre, Brazil
[8]Also at University of Chinese Academy of Sciences, Beijing, China
[9]Also at China Center of Advanced Science and Technology, Beijing, China
[10]Also at University of Chinese Academy of Sciences, Beijing, China
[11]Also at China Spallation Neutron Source, Guangdong, China
[12]Now at Henan Normal University, Xinxiang, China
[13]Also at University of Shanghai for Science and Technology, Shanghai, China
[14]Now at The University of Iowa, Iowa City, Iowa, USA
[15]Also at an institute formerly covered by a cooperation agreement with CERN
[16]Also at Zewail City of Science and Technology, Zewail, Egypt
[17]Also at British University in Egypt, Cairo, Egypt
[18]Now at Ain Shams University, Cairo, Egypt
[19]Also at Purdue University, West Lafayette, Indiana, USA
[20]Also at Université de Haute Alsace, Mulhouse, France
[21]Also at Istinye University, Istanbul, Turkey
[22]Also at The University of the State of Amazonas, Manaus, Brazil
[23]Also at University of Hamburg, Hamburg, Germany
[24]Also at RWTH Aachen University, III. Physikalisches Institut A, Aachen, Germany
[25]Also at Bergische University Wuppertal (BUW), Wuppertal, Germany
[26]Also at Brandenburg University of Technology, Cottbus, Germany
[27]Also at Forschungszentrum Jülich, Juelich, Germany
[28]Also at CERN, European Organization for Nuclear Research, Geneva, Switzerland
[29]Also at HUN-REN ATOMKI - Institute of Nuclear Research, Debrecen, Hungary
[30]Now at Universitatea Babes-Bolyai - Facultatea de Fizica, Cluj-Napoca, Romania
[31]Also at MTA-ELTE Lendület CMS Particle and Nuclear Physics Group, Eötvös Loránd University, Budapest, Hungary
[32]Also at HUN-REN Wigner Research Centre for Physics, Budapest, Hungary
[33]Also at Physics Department, Faculty of Science, Assiut University, Assiut, Egypt
[34]Also at Punjab Agricultural University, Ludhiana, India
[35]Also at University of Visva-Bharati, Santiniketan, India
[36]Also at Indian Institute of Science (IISc), Bangalore, India
[37]Also at Amity University Uttar Pradesh, Noida, India

[38]Also at UPES - University of Petroleum and Energy Studies, Dehradun, India
[39]Also at IIT Bhubaneswar, Bhubaneswar, India
[40]Also at Institute of Physics, Bhubaneswar, India
[41]Also at University of Hyderabad, Hyderabad, India
[42]Also at Deutsches Elektronen-Synchrotron, Hamburg, Germany
[43]Also at Isfahan University of Technology, Isfahan, Iran
[44]Also at Sharif University of Technology, Tehran, Iran
[45]Also at Department of Physics, University of Science and Technology of Mazandaran, Behshahr, Iran
[46]Also at Department of Physics, Faculty of Science, Arak University, ARAK, Iran
[47]Also at Helwan University, Cairo, Egypt
[48]Also at Italian National Agency for New Technologies, Energy and Sustainable Economic Development, Bologna, Italy
[49]Also at Centro Siciliano di Fisica Nucleare e di Struttura Della Materia, Catania, Italy
[50]Also at Università degli Studi Guglielmo Marconi, Roma, Italy
[51]Also at Scuola Superiore Meridionale, Università di Napoli 'Federico II', Napoli, Italy
[52]Also at Fermi National Accelerator Laboratory, Batavia, Illinois, USA
[53]Also at Lulea University of Technology, Lulea, Sweden
[54]Also at Laboratori Nazionali di Legnaro dell'INFN, Legnaro, Italy
[55]Also at Consiglio Nazionale delle Ricerche - Istituto Officina dei Materiali, Perugia, Italy
[56]Also at Institut de Physique des 2 Infinis de Lyon (IP2I), Villeurbanne, France
[57]Also at Department of Applied Physics, Faculty of Science and Technology, Universiti Kebangsaan Malaysia, Bangi, Malaysia
[58]Also at Consejo Nacional de Ciencia y Tecnología, Mexico City, Mexico
[59]Also at Trincomalee Campus, Eastern University, Sri Lanka, Nilaveli, Sri Lanka
[60]Also at Saegis Campus, Nugegoda, Sri Lanka
[61]Also at National and Kapodistrian University of Athens, Athens, Greece
[62]Also at Ecole Polytechnique Fédérale Lausanne, Lausanne, Switzerland
[63]Also at Universität Zürich, Zurich, Switzerland
[64]Also at Stefan Meyer Institute for Subatomic Physics, Vienna, Austria
[65]Also at Laboratoire d'Annecy-le-Vieux de Physique des Particules, IN2P3-CNRS, Annecy-le-Vieux, France
[66]Also at Near East University, Research Center of Experimental Health Science, Mersin, Turkey
[67]Also at Konya Technical University, Konya, Turkey
[68]Also at Izmir Bakircay University, Izmir, Turkey
[69]Also at Adiyaman University, Adiyaman, Turkey
[70]Also at Bozok Universitetesi Rektörlügü, Yozgat, Turkey
[71]Also at Marmara University, Istanbul, Turkey
[72]Also at Milli Savunma University, Istanbul, Turkey
[73]Also at Kafkas University, Kars, Turkey
[74]Now at Istanbul Okan University, Istanbul, Turkey
[75]Also at Hacettepe University, Ankara, Turkey
[76]Also at Erzincan Binali Yildirim University, Erzincan, Turkey
[77]Also at Istanbul University - Cerrahpasa, Faculty of Engineering, Istanbul, Turkey
[78]Also at Yildiz Technical University, Istanbul, Turkey
[79]Also at School of Physics and Astronomy, University of Southampton, Southampton, United Kingdom
[80]Also at IPPP Durham University, Durham, United Kingdom

[81]Also at Monash University, Faculty of Science, Clayton, Australia
[82]Also at Università di Torino, Torino, Italy
[83]Also at Bethel University, St. Paul, Minnesota, USA
[84]Also at Karamanoğlu Mehmetbey University, Karaman, Turkey
[85]Also at California Institute of Technology, Pasadena, California, USA
[86]Also at United States Naval Academy, Annapolis, Maryland, USA
[87]Also at Bingol University, Bingol, Turkey
[88]Also at Georgian Technical University, Tbilisi, Georgia
[89]Also at Sinop University, Sinop, Turkey
[90]Also at Erciyes University, Kayseri, Turkey
[91]Also at Horia Hulubei National Institute of Physics and Nuclear Engineering (IFIN-HH), Bucharest, Romania
[92]Now at another institute formerly covered by a cooperation agreement with CERN
[93]Also at Texas A&M University at Qatar, Doha, Qatar
[94]Also at Kyungpook National University, Daegu, Korea
[95]Also at Yerevan Physics Institute, Yerevan, Armenia
[96]Also at another institute formerly covered by a cooperation agreement with CERN
[97]Also at Imperial College, London, United Kingdom
[98]Also at Institute of Nuclear Physics of the Uzbekistan Academy of Sciences, Tashkent, Uzbekistan